



JOHANNES KEPLER
UNIVERSITÄT LINZ
Netzwerk für Forschung, Lehre und Praxis



Synthesis and Characterisation of CuInS₂-Nanoparticles for Hybrid Solar Cells

Diplomarbeit zur Erlangung des akademischen Grades

Diplom Ingenieur

im Diplomstudium

Wirtschaftsingenieurwesen - Technische Chemie

angefertigt am

Linz Institute for Organic Solar Cells (LIOS)

eingereicht von

Sandra Hofer

unter der Betreuung von

o. Univ. Prof. Dr. Serdar N. Sariciftci

Linz, Juli 2005

Johannes Kepler Universität Linz

A-4040 Linz • Altenbergerstraße 69 • Internet: <http://www.jku.at> • DVR 0093696

To my parents
Lotte und Wolfgang

Zusammenfassung

Es wurden Hybrid Solarzellen mit CuInS₂-Nanopartikeln und unterschiedlichen organischen Materialien (Poly - 3 - hexylthiophen, 1 - (3 - methoxycarbonyl) propyl - 1 - phenyl [6,6]C₆₁) untersucht. Die CuInS₂-Nanopartikel wurden über einen kolloidalen Ansatz synthetisiert. Mittels Röntgendiffraktion wurden die Partikel qualitative analysiert. Zur Bestimmung der Partikelgröße wurde Transmission Elektronen Mikroskopie (TEM) angewandt. Die Größe liegt bei 20 bis 500 nm. Die einzelnen Schichten wurden mittels AFM (Atomic Force Microscopy) untersucht.

Die besten Ergebnisse wurden bei Zweischicht - Solarzellen aus CuInS₂ und 1 - (3 - methoxycarbonyl) propyl - 1 - phenyl [6,6]C₆₁ (PCBM) erreicht. Weiters wurde das synthetisierte CuInS₂ für Pufferschichten in sogenannten CISCuT Solarzellen benutzt. Effizienzen von 0.1% wurden erreicht.

Abstract

Hybrid solar cells using CuInS₂-nanoparticles mixed with different organic materials (poly - 3 - hexylthiophen, 1 - (3 - methoxycarbonyl) propyl - 1 - phenyl [6,6]C₆₁) were investigated. The CuInS₂-nanoparticles were synthesised via a colloidal route. The particles were qualitatively analyzed with X-ray. Transmission electron spectroscopy (TEM) was done to determine the size of the particles, that ranges between 20 and 500 nm. The layers were investigated by AFM (Atomic Force Microscopy).

The best results were achieved with CuInS₂ / 1 - (3 - methoxycarbonyl) propyl - 1 - phenyl [6,6]C₆₁ (PCBM) bilayer heterojunction solar cells. Furthermore the synthesised CuInS₂ was used as buffer layer in so called CISCuT solar cells. Efficiencies up to 0.1 % were achieved.

Table of Contents

Acknowledgement	4
1 Introduction.....	5
1.1 World Energy Demand and the Necessity of Alternative Energy Sources ...	5
1.2 Hybrid Solar Cells with Core/Shell Nanomaterials.....	6
1.3 Aim of this Thesis	8
1.4 CuInS ₂ Hybrid Solar Cells	8
1.5 Theory	10
1.6 Energy Levels of the used Materials	16
2 Experimental	17
2.1 Synthesis.....	17
2.1.1 Equipment.....	18
2.1.2 Reactants and other used Reagents.....	20
2.2 X-ray - Spectroscopy.....	21
2.3 Transmission Electron Microscopy Measurements	23
2.4 Device Preparation.....	25
2.4.1 Solar Cell Schemata	25
2.4.2 Substrate Preparation	28
2.4.3 CIS Layers in Bilayer Solar Cells and CISCuT - Solar Cell	29
2.4.4 PCBM Layer in Bilayer Solar Cells.....	29
2.4.5 P3HT Layers in Bilayer Solar Cells	30
2.4.6 PEDOT:PSS Layers.....	31
2.4.7 Mixed Layers of CIS and PCBM or P3HT in Bulk Heterojunction Cells	32
2.4.8 Top Contact Evaporation	32
2.5 AFM Measurements	33
2.6 Current-Voltage Measurements	33
2.7 IPCE Measurements	35
3 Results and Discussion	36
3.1 Changes in the Synthesis.....	36
3.2 X- Ray Spectroscopy.....	38
3.3 TEM.....	41
3.4 AFM Measurements	44

3.4.1	Substrates and PEDOT:PSS.....	44
3.4.2	Single Layers of PCBM, P3HT and CIS	46
3.4.3	Bulk Heterojunction Solar Cells.....	48
3.4.4	Bilayer Solar Cells.....	50
3.5	Examples for Solar Cells	52
3.5.1	Bilayer Solar Cells.....	52
3.5.2	Bulk Heterojunction Solar Cells.....	55
3.5.3	CISCuT Solar Cells	55
3.6	IPCE Measurements	57
4	Conclusion.....	58
	Curriculum Vitae	64
	Eidesstattliche Erklärung	66

Acknowledgement

First I would like to thank my whole family, especially my parents and grandparents, who always supported me during the years of my studies. Unfortunately not all of you could witness the end of my studies.

Special thanks go to my supervisors Dr. Helmut Neugebauer and o. Univ. Prof. Dr. Serdar Sariciftci.

Furthermore I want to thank:

Serap Gunes for her help and understanding when I did not know how to go on and for helping me with the AFM pictures. Gebi Matt, who was my supervisor during my internship at the institute, and the expert for any question concerning physics.

And the other 3 “Spice Girls”: Anita Fuchsbauer, Christina Mitterbauer, Linda Wildling – who accompanied me during my studies!

Special thanks go to Petra Neumaier, our secretary, who helped me to survive in the administrative jungle of the university and Manfred Lipp for building me my own little N₂ – glovebox and for his help with other technical problems.

Also I would like to thank Elif Arici (Siemens, Erlangen, Germany) for her help with the synthesis and Sergei Bereznev (Tallinn University of Technology, Tallinn, Estonia) for the collaboration concerning the CISCuT solar cells. I would like to thank O. Univ.-Prof. Mag. Dipl.-Ing. Dr. Gerhard Gritzner and Mr. Karl Kellner from the Institute for Chemical Technology of Inorganic Materials, Johannes Kepler Universität Linz for the X-ray analysis.

And my thanks goes to all the (former) staff of LIOS:

(Elke Bradt), Erika Bradt, (Luis Campos), Gilles Dennler, (Martin Dress), (Berndt Ebner), Martin Egginger, (Alexander Gusenbauer), Gerda Kalab, Robert Köppe, Sheng Li Lu, Christoph Lungenschmied, Nenad Marjanovic, Farideh Meghdadi, (Attila Mozer), Le Hong Nguyen, (Birgit Paulik), Hans-Jürgen Prall, (Alia Selim), Birendra Singh and (Christoph Winder).

1 Introduction

1.1 *World Energy Demand and the Necessity of Alternative Energy Sources*

The world energy demand is still increasing. At the moment fossil fuels and nuclear energy are the main energy sources. This classical energy sources cannot provide us with enough energy for the future any more. One problem is that the resources are limited. The stock of carbon-based fuels will be exploited in roughly 50 years. Another big problem is that carbon dioxide, the final product of burned fossil fuel, is known to influence earth climate significantly. Nuclear energy has always been subject of intensive public discussion due to the security and health risks of nuclear power stations and the following problems with radioactive waste.

To solve these problems, big efforts have been made to develop new, alternative energy sources over the last decades.

One of this alternative energy sources is solar energy. The sun is the ideal energy source. It is reliable, clean, for free and can be used all over the world.

The direct conversion of sunlight into electricity by photovoltaic cells is widely used in the meantime. In Austria photovoltaic modules with a power output of 16 823 kW (peak) have been installed till the end of 2003. The main part of the installed modules is based on silicon. The production costs of silicon solar cells are high due to the very energy intensive production. Therefore thin film technique should reduce material consumption and production costs. For these techniques inorganic semiconductors like amorphous or polycrystalline silicon, cadmium telluride or copper indium diselenide and disulphide or organic semiconductors can be used. For organic solar cells or hybrid solar cells very cheap coating techniques like spin coating, doctor blading, ink jet printing, etc. are available.

Until now no organic or hybrid solar cells are on the market. However Siemens announced to be able to produce organic solar cells with 5 % efficiency by printing on flexible substrates .

1.2 Hybrid Solar Cells with Core/Shell Nanomaterials

Nanoclusters of inorganic semiconductors have been subject of increased research in the last years. This is mainly due to the size dependent new properties of these materials. The photo-emission and absorption of semiconductor nanocrystals is tuneable by the size as a result of quantum confinement effects. The problem is that very small inorganic crystals are generally unstable due to their high surface tension, and thus have a tendency to transform to large particles by Ostwald ripening. Therefore nanoparticles shielded by an organic ligand, so called “core-shell” particles, were created. This shell cannot only avoid the aggregation and oxidation of the particles, but also can alter the dispersion characteristics of the particles by surface modification, so that the possibility is given to blend core/shell particles into the polymer matrices, so called hybrid materials.

Typically, inorganic semiconductors in macroscopic dimensions, irrespectively of their size, will absorb all electromagnetic radiation with an energy greater than the band gap. If the particles become smaller than the size of the exciton in the bulk semiconductor, their electronic structure changes. The electronic properties of such a small particle are hence more like those of a giant molecule than an extended solid. The properties will depend not only on the material, but also on their size [1-5]. The lowest energy of optical transition, among others, will increase significantly due to the quantum confinement with decreasing size of the inorganic cluster. As hybrid solar cells are cells made of inorganic nanocrystals mixed with organic materials (mostly polymers) new possibilities for the tailoring of solar cells arise. With the option to change the energy level of the nanoparticles through size dependence and since the energy levels of the polymers can be tuned by chemical modification of the backbone-chain, it is possible for blends with the two materials to tailor optimal conditions for a solar cell including energy gain from charge transfer for the efficient charge separation and the spectral range of the absorbing light.

There are two possibilities to make hybrid solar cells: bilayer cells or bulk heterojunction solar cells. In bilayer solar cells a layer of a p-type material is produced on top or under a layer of an n-type material. In bulk heterojunction

solar cells a high concentration of the nanoparticles are blended in an organic matrix, to form an interpenetrating network.

Hybrid solar cells were fabricated from blends of nanocrystals with semiconducting polymers as a photovoltaic layer. P-n-junction by using a p-doping semiconducting polymer (poly - 3 - hexylthiophenes, poly(2 - methoxy,5 - (2'-ethoxy) - hexyloxy - *p* - phenylenevinylene) and n-type II-VI semiconductor nanoparticles (CdSe, CuInSe₂,...) were reported from different groups [6-9].

Another possibility is to use p-type semiconductor nanoparticles like CuInS₂ and n-type organic materials like PCBM [10].

The reasons for hybrid solar cells are easily described: Most of the cheap and easy techniques for organic solar cells can also be used for hybrid solar cells. The advantage of inorganic nanomaterials is that the semiconductors have a higher absorption range and photoconductivity than organic materials. The doping level of the inorganic nanocrystalline semiconductors can easily be varied by synthesis and the stoichiometry [11].

One problem with hybrid solar cells is that often the charge transport through the nanoparticle-polymer interface is poor because the nanocrystals are surrounded by the ligand shell. This shell is limiting the transport. A better charge carrier exchange can be realized if it is possible to wash away the ligands.

1.3 Aim of this Thesis

In this thesis hybrid solar cells with CuInS₂, P3HT and PCBM are investigated. The fabrication of CuInS₂ was done by a colloidal route. The produced particles were evaluated in hybrid solar cells. An important concern was to find the best parameters for the synthesis. The synthesised particles should be easily processable for solar cells. Furthermore the p- or n-type characteristic of the material should be changed by changing the stoichiometry.

The particles were investigated by X-Ray and transmission electron microscopy. The built layers were investigated by Atomic Force Microscopy.

A main goal was to build solar cells with these nanoparticles and to characterise them. Therefore current - voltage curves and incident-photon-to-current-efficiency (IPCE)-measurements were done.

Also CuInS₂ nanoparticles were used as a buffer layer in CISCuT solar cells.

In chapter 1 the basics of hybrid solar cells were discussed and in the following sub-section the theory of hybrid solar cells for this thesis will be described briefly. In chapter 2 the synthesis of the nanoparticles, device preparation, the material and measurement setups used in these studies are explained. Chapter 3 contains the results of the investigations altogether with the discussion of the results. The work finishes with a short conclusion.

1.4 CuInS₂ Hybrid Solar Cells

Some important studies on CIS hybrid solar cells will be listed.

For a device of ITO / PEDOT : PSS / CIS / LiF / Al a short-circuit current (j_{SC}) of 0.02 mA cm⁻² and an open-circuit voltage (V_{OC}) of 450 mV have been reported by Arici et al. [10] This devices had a rectification ratio (RR) of 2.5 (at ± 2 V) and a FF of 0.25.

In this publication [10] also of a CIS/PCBM bilayer cell was reported. The j_{SC} was 0.26 mA cm⁻² and the V_{OC} was 710 – 790 mV, the FF was 0.44 and the conversion efficiency 0.086%, the RR in the dark was 2.5.

In another paper by Arici et al. [12] a ITO / CIS : PEDOT : PSS / LiF / Al bulkheterojunction cell was reported. The j_{SC} was 0.004 mA cm⁻² and the V_{OC} 150 mV, the FF was 0.1 and the conversion efficiency 0.003%, the RR in the dark was 2.2. In these cells an additional PCBM interlayer was introduced: The j_{SC} was 0.84 mA cm⁻² and the V_{OC} was 220 mV, the RR in the dark was 13.1.

1.5 Theory

The working principles of hybrid solar cells can partially be explained with the theory of organic solar cells. Therefore the theory for organic solar cells will now be explained.

To convert light into electric current in solar cells four steps have to be run through:

- Absorption of light, leading to an excited state, the electron hole pair (exciton)
- Exciton diffusion
- Charge separation at an interface
- Charge transport to the anode (holes) and cathode (electrons) [13]

A pair of separated positive and negative charges stores a potential energy that is equivalent to the difference in their respective quasi-Fermi level. It is corresponding to the difference in the electrochemical potentials. [14]

The electric current delivered by a photovoltaic solar cell corresponds to the number of created charges that are collected at the electrode. This number is a product of the photons that are absorbed, the electron hole pairs that are dissociated and the charges which reach the electrodes.

The charges need a net driving force to reach the electrode. Generally this results from a gradient in the electrochemical potential of electrons and holes. This is done by two “forces”: the internal electric field, which leads to a field induced drift, and the concentration gradient of the respective charge carrier species, which leads to a diffusion current. Generally it can be said that in thin film devices (<100 nm) the field drift dominates, whereas in thick devices the diffusion of the charge carriers is dominated by concentration gradients. [13]

To understand the behaviour of a nondoped semiconductor device in the dark the MIM (metal-insulator-metal) [15] model is of great importance: Figure 1 shows a semiconductor between two metal electrodes with different workfunctions. The metals are represented by their Fermi levels, and the semiconductors by their valence band and conduction band, corresponding to the molecular LUMO

(lowest unoccupied molecular orbital) and the HOMO (highest occupied molecular orbital).

Figure 1a) shows the closed circuit condition (no voltage is applied). In the dark no net current is flowing and the built-in electric field resulting from the differences in the metals' work function is evenly distributed throughout the device. Under illumination, separated charge carriers can drift in this electric field to the respective contacts, the device works then as a solar cell. Figure 1b) shows the situation for the open circuit or flat band condition. The applied voltage is called open circuit voltage V_{OC} . It corresponds to the differences in the metals' work functions. There is no net driving force for the charge carriers, therefore the current is zero. In Figure 1c) a reverse bias is applied. Only a very small injected dark current can flow. Under illumination the generated charge carriers drift under a strong electric field to the respective electrodes and the diode works as a photodetector. In Figure 1d) the applied forward bias is larger than the open circuit voltage. The contacts can efficiently inject charges into the semiconductor. The device works as a LED if the charges recombine radiatively. The asymmetric diode behaviour results basically from the different injection of the two metals into the HOMO and LUMO levels. [13]

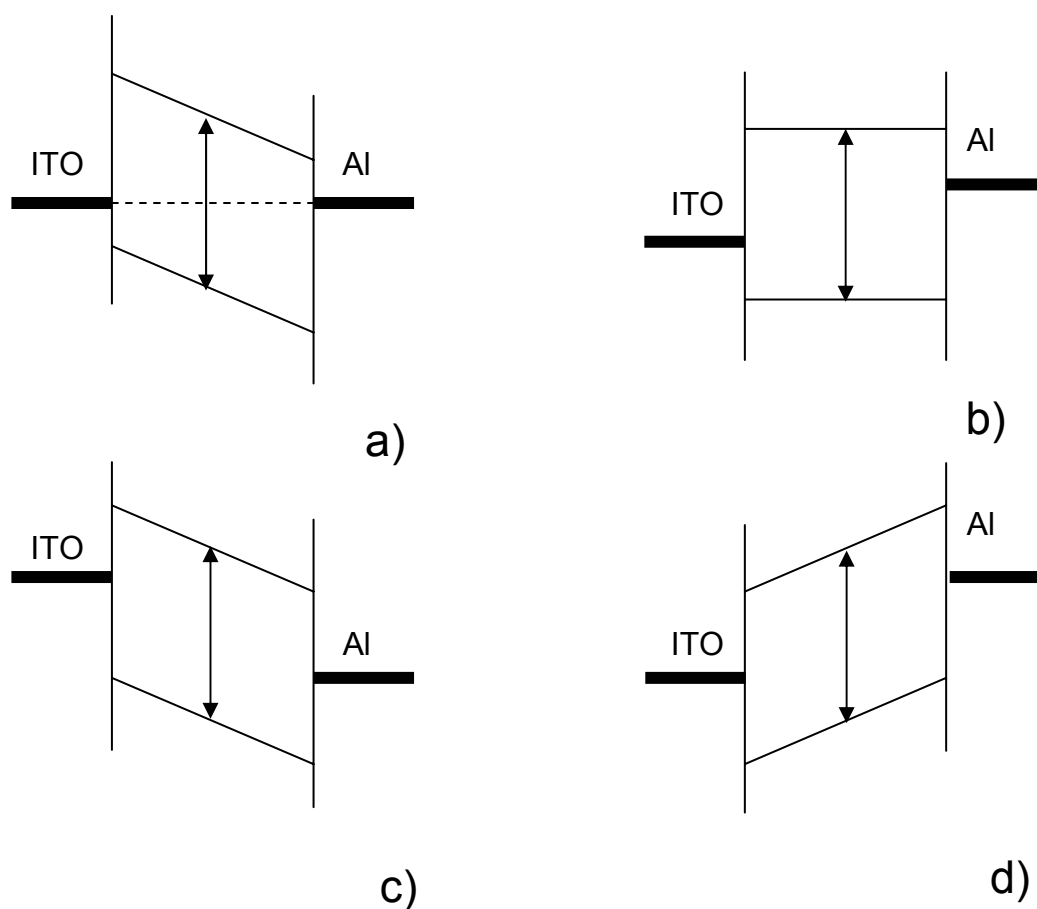


Figure 1: MIM picture: a) Closed circuit condition: under illumination photogenerated charged drift towards contacts. b) open circuit condition: the current becomes zero. c) reversed bias: the diode operates as photodetector d) forward bias larger than V_{OC} : the injection increases and the diode opens up

Single Layer Devices

These devices consist of a molecular organic layer sandwich between two metal electrodes of different work functions. It can be explained by the MIM-model (for insulator) or by the formation of a Schottky barrier (for doped materials) between the metal with the lower workfunction and the p-type organic layer.

Figure 2 shows a scheme for a single layer device with a Schottky junction at the aluminium contact. Close to the contact, in the depletion region W , a resulting band bending from the Schottky contact is depicted. This corresponds to an electric field in where excitons can be dissociated. [16]

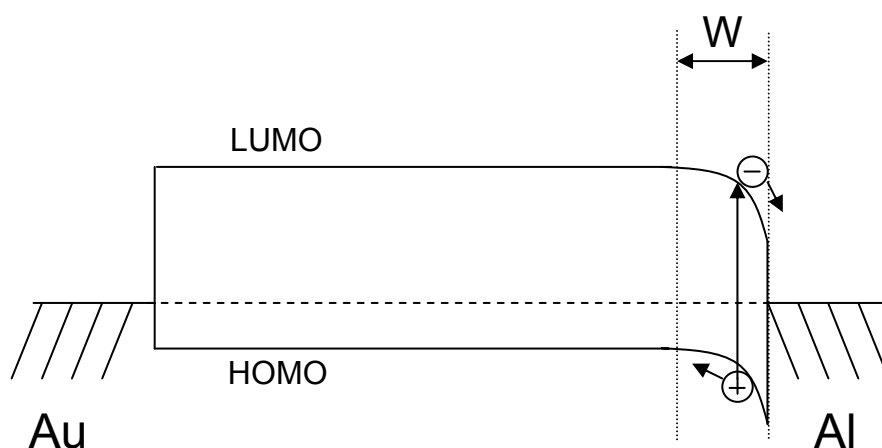


Figure 2: Single layer device with a Schottky contact at the Al contact.

Bilayer Heterojunction

In this device a donor and an acceptor material are stacked together with an planar interface. Due to the large potential drop between donor and acceptor at the interface charge separation occurs. [17-20] The two electrodes of the bilayer have to match the donor HOMO and the acceptor LUMO, otherwise no efficient extraction of the charge carriers is possible.

Figure 3 shows the schematic of a bilayer heterojunction device, neglecting all kinds of possible band bending due to energy alignment. The charge transfer in bilayer heterojunction between undoped donor and acceptor materials is due to the differences in the ionization potential and electron affinity of the adjacent materials. It can be compared with the classical p/n-junction. Upon photon absorption in the donor D, the electrons are excited from the HOMO to the LUMO - state ($S^0 \rightarrow S^1$).

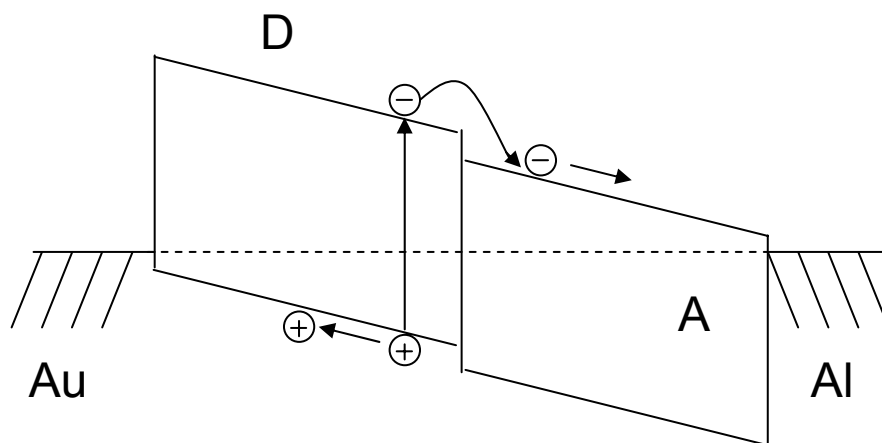


Figure 3: Schematic of a bilayer heterojunction device. The Donor (D) contacts the higher and the acceptor (A) the lower work function metal.

If an acceptor molecule A is in close proximity, the electron may be transferred to the LUMO of A, which is energetically preferred when:

$$I_{D^*} - A_A - U_C < 0$$

I_{D^*} is the ionization potential of the excited state of the donor, A_A the electron affinity of the acceptor and U_C effective Coulomb interaction. [21]

The realising electron energy may then be used to separate electrons and holes from their Coulomb potential. This photoinduced charge transfer only occurs under illumination, because the illumination is needed to gain the excitation energy of the electron in the donor to reach the LUMO in the acceptor. Experiments [16, 22, 23] and also theoretical considerations [24] indicate a formation of an interfacial dipole between the donor and acceptor phase, independent of illumination. This can stabilize the charge-separation state by a repulsive interaction between the interface and the free charge [24]. Therefore the charge separated state is very stable. The recombination rate between holes in D and electrons in A is several orders of magnitude smaller than the forward charge transfer rate [25, 26, 27].

Bulk Heterojunction

The basic principle is to mix the donor and the acceptor materials intimately in a bulk volume so that each donor-acceptor interface is within a distance less than the exciton diffusion length of each absorbing site.

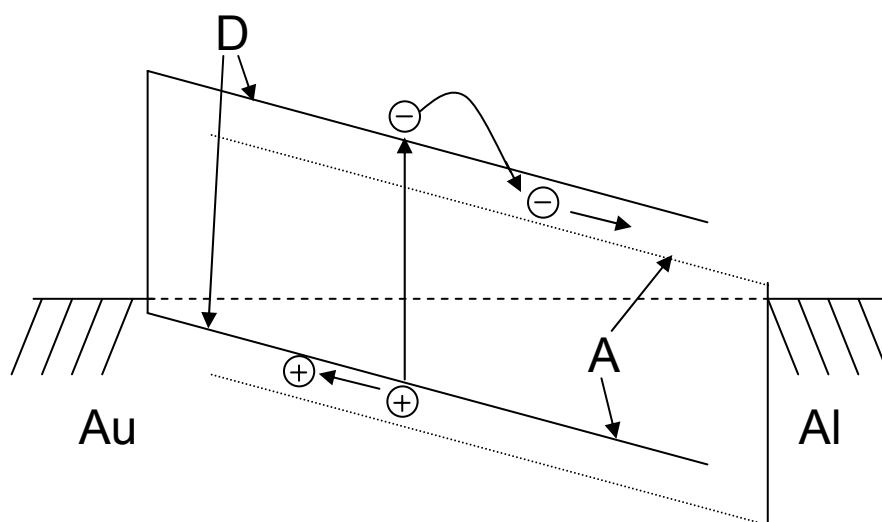


Figure 4: Schematic of a bulk heterojunction device. The donor (D) is blended with the acceptor (A) throughout the whole film.

Figure 4 shows a bulk heterojunction device, again neglecting all kinds of energy level alignment and interface effects. With respect to the D-A concept the heterojunction device is similar to the bilayer device, but it exhibits a largely increased interfacial area where charge separation occurs. No loss due to too small exciton diffusion length is expected, because of the interfaces being dispersed throughout the bulk. Ideally all excitons will be dissociated within their lifetime. The charges in this conception are also separated within the different phases. Therefore the recombination is reduced to a large extent and the photocurrent often follows the light intensity. Different from the bilayer heterojunction in bulk heterojunction percolated pathways for the holes and the electron transporting phases to the contacts are required. It requires, that once the electrons and holes are separated into different materials, each carrier type has a pathway to the appropriate electrode without needing to pass through a

region of the other material [28]. Also the nanoscopic morphology of the composite layer plays a fundamental role for the solar cell. Phase separation should be avoided. [29]

1.6 Energy Levels of the used Materials

The nature of a contact between a semiconductor and a metal or between two semiconductors is given by the workfunctions: the energetic difference between the Fermi levels and the vacuum level.

Figure 5 shows the workfunctions for ITO, PEDOT : PSS, Al and Au together with the HOMO and LUMO levels for P3HT, CIS and PCBM. The HOMO and LUMO levels for macroscopic CIS are approximately - 5.6 eV and - 4.1 eV. Because of the size distribution of the quantized CIS particles, a distribution of their energy gaps must be expected. [12]

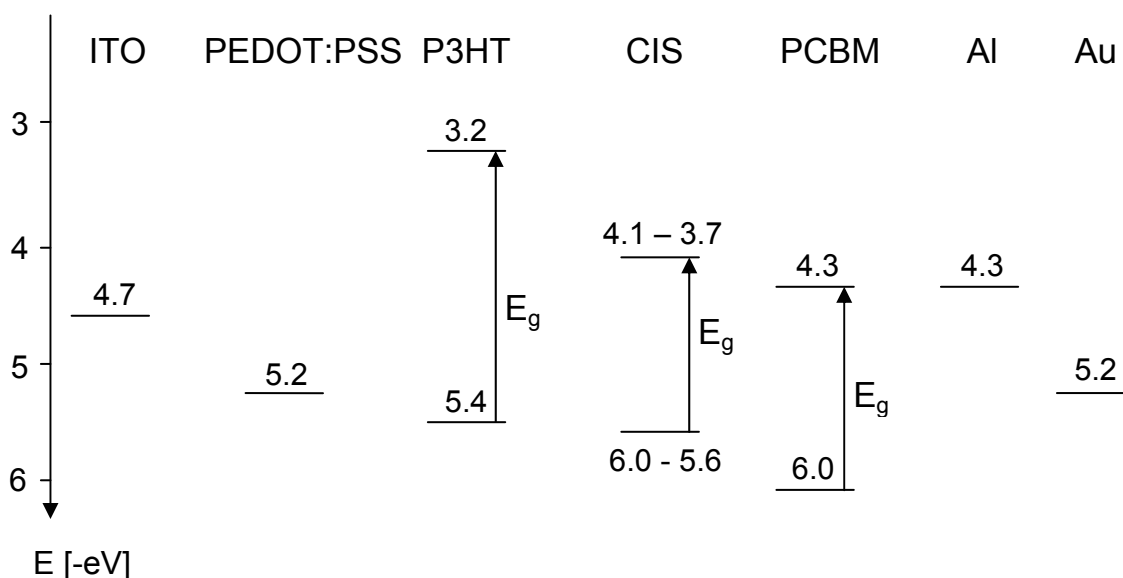


Figure 5: Energy levels of the investigated materials.

2 Experimental

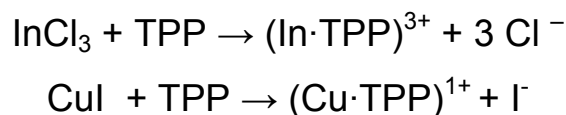
2.1 Synthesis

For the wet-chemical synthesis of CuInS₂ – nanoparticles different way of synthesis can be used: a hydrothermal and a colloidal route. Here the colloidal route was performed. Also different organic surfactants can be used, like Triphenylphosphite [30], Tri-*n*-octylphosphine oxide [31], Hexadecylamine [32] or other phosphines and primary amines. Here only Triphenylphosphite (TPP) was used.

The synthesis was done as described in the paper of Czekelius et al [30] or Arici et al. [12].

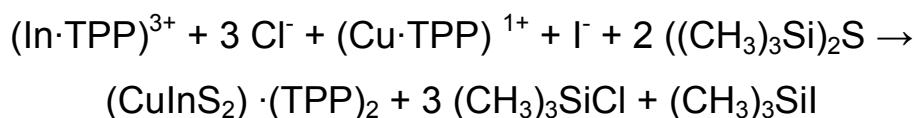
The reaction was carried out in two steps:

1. Step:



4.4 g (0.02 mol) InCl₃ were suspended in a solution of 200 ml acetonitrile and 10 ml (0.04 mol) TPP. The suspension was refluxed in a 500 ml three-neck flask in an argon atmosphere with magnetic stirring for 2 hours to produce a homogeneous InCl₃ - TPP solution. In a separated 500 ml three-neck flask 3.7 g (0.02 mol) CuI were added to a solution of 200 ml acetonitrile and 15 ml (0.06 mol) TPP. This solution was also refluxed under stirring for 2 hours under argon atmosphere. After 2 hours both solutions were cooled down to room temperature.

2. Step:



Then the solutions were mixed together and purged with argon. Bis(trimethylsilyl)sulfide mixed with TPP was then added dropwise within 2 hours. The colour changed from colourless over yellow and orange to red.

With the last synthesis this step was done in a home made N₂-glovebox.

The equipment used for the synthesis can be seen in Figure 6 and Figure 7.

2.1.1 Equipment

Equipment used for the first step of the reaction:

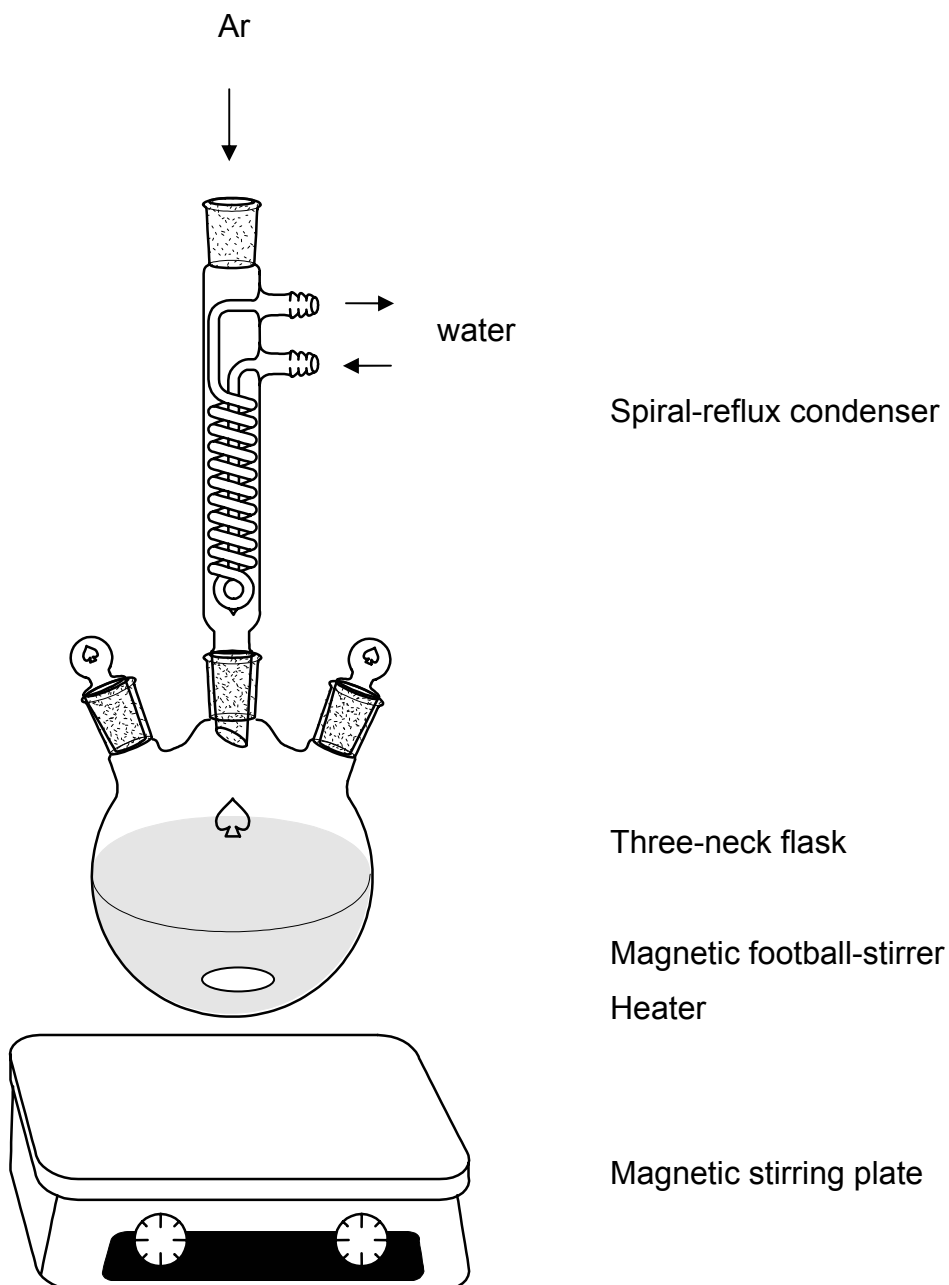


Figure 6: Equipment for the first step of the reaction

Equipment used for the second step of the reaction:

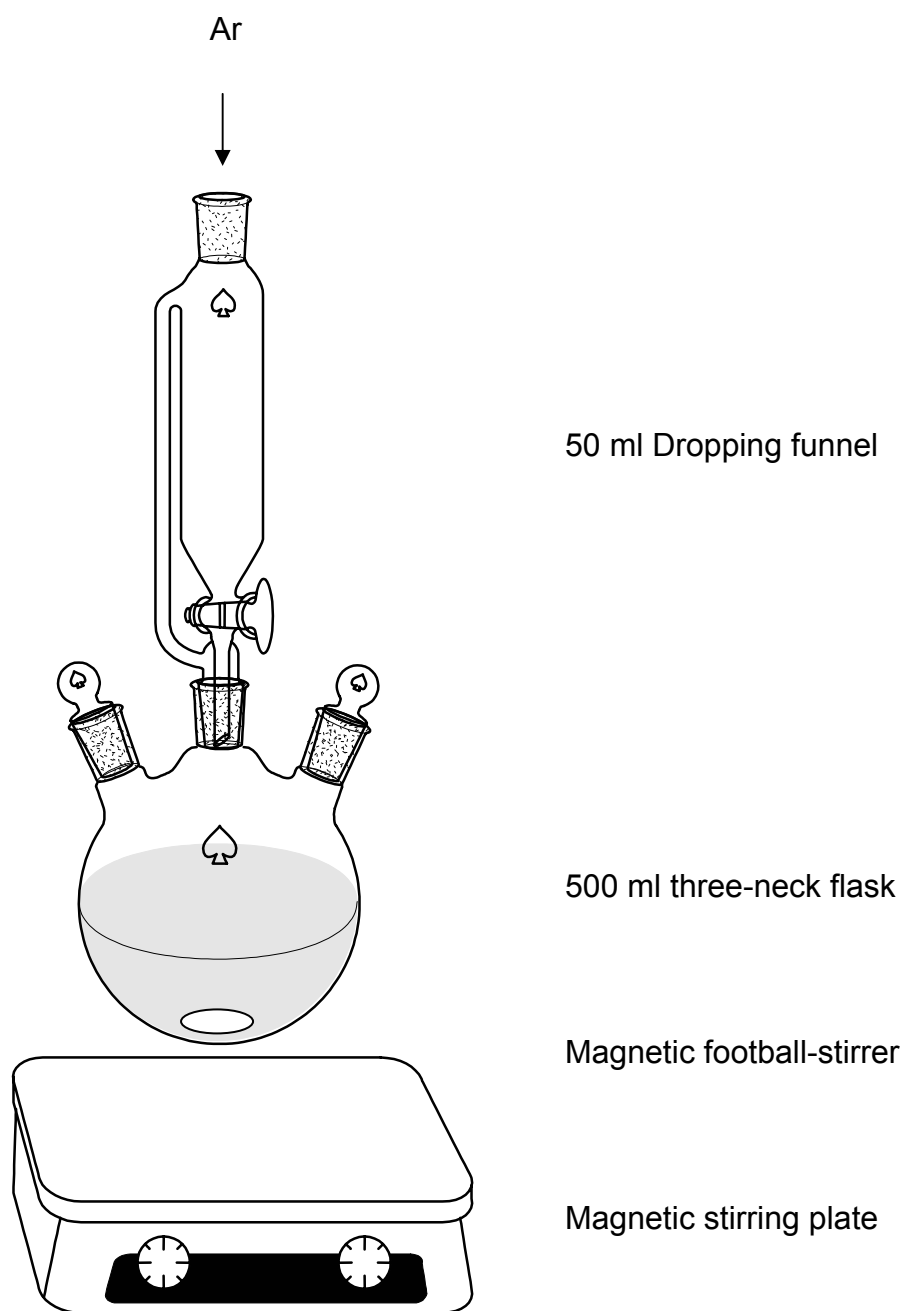


Figure 7: Equipment for the second step of the reaction

2.1.2 Reactants and other used Reagents

Indium(III)chloride

Sigma-Aldrich, 99.999 %, InCl₃ MW: 220.35 g mol⁻¹

Copper(I)iodine

Sigma-Aldrich, 99,999 %, CuI, MW: 190.44 g mol⁻¹

Triphenylphosphite

Sigma-Aldrich, 97 %, ((C₆H₅O)₃P), MW: 310.27 g mol⁻¹,

Phosphonigesäure - triphenylester

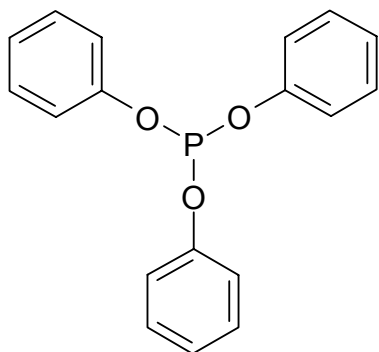


Figure 8: Chemical structure of Triphenylphosphite

Bis(trimethylsilyl)sulfide

Sigma-Aldrich, ((CH₃)₃Si)₂S, MW: 179.75 g mol⁻¹,

1, 1, 1, 3, 3, 3 – Hexamethyldisilathian

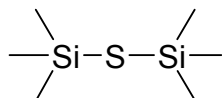


Figure 9: Chemical structure of Bis(trimethylsilyl)sulfide

Acetonitrile

Sigma-Aldrich, 99,8 % anhydrous, CH₃CN, MW: 119.5 g mol⁻¹

2.2 X-ray - Spectroscopy

With X-ray-diffraction it is possible to identify the distances of the crystal lattice planes. Therefore it is possible to analyze substances qualitatively and quantitatively. In this thesis X-ray-diffraction was used to identify CuInS₂ qualitatively.

The measuring principle is based on the reflection, respectively diffraction of X-ray. To generate monochromatic X-ray a β -filter (in case of Cu_{K α} , a nickel-filter) is used. It filters the bremspectrum and all the other not used X-Ray lines out from the emitted spectrum of the X-ray source (in the majority of cases a copper anode). If one of this monochromatic X-ray hits the sample, parts of the X-ray will be absorbed and others will be reflected, respectively diffracted. Due to the diffraction the overlapping of waves happens. Depending on the geometrical orientation the overlapping leads to amplification or erasement. If the Bragg Equation (Equation 1) is fulfilled a maximum of the intensity is detected with the counter. In Figure 10 a schematic configuration of a conventional X-ray diffraction machine can be seen.

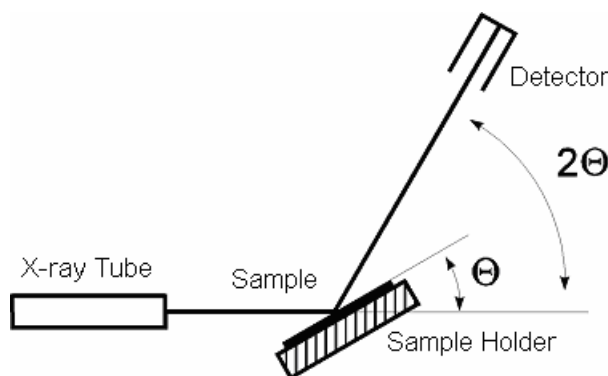


Figure 10: Configuration of a X-ray diffraction machine [33]

The X-ray hits the sample under an adjustable angle θ . The intensity of the reflected beam is measured with the detector. The detector moves with a varying glancing angle θ on the measuring circuit in the way that the angle between the beam direction and the detector is always 2θ .

Bragg Equation:

X-ray-reflexes can only be detected if any lattice plane with the Miller indices $(h k l)$ fulfills the Bragg equation [34]:

Equation 1
$$n * \lambda = 2 * d_{hkl} * \sin \Theta$$

norder

λwavelength of Cu-K α -radiation

d_{hkl}distance between two lattice planes

θused glancing angle

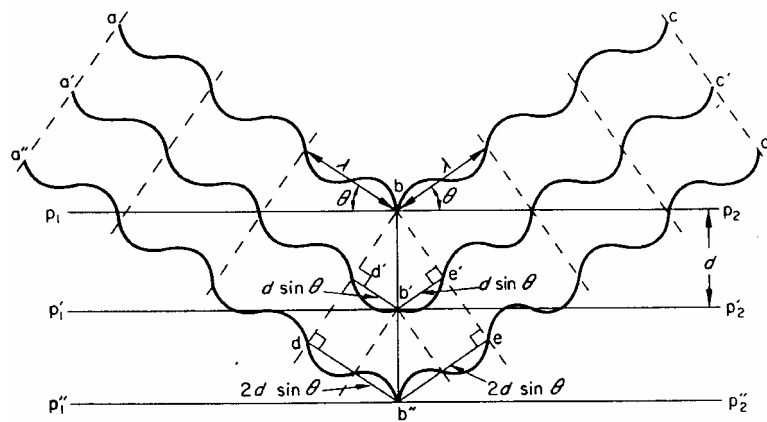


Figure 11: Condition for diffraction of X-ray radiation

The measured spectra show maxima of intensity at certain angles. The phases inside the sample can be identified and the maxima can be assigned, by comparing the spectra to references from the JCPDS data and with theoretically calculated diffractograms. For the measurement in this thesis an X'Pert Pro Röntgendiffraktometer (Phillips) has been used. The X-ray analyses were done by Mr. Karl Kellner.

2.3 Transmission Electron Microscopy Measurements

A Transmission Electron Microscope (TEM) (Jeol 2012 FasTEM, Jeol, Tokyo, J) was used to estimate the size of the particles. The solution of CuInS₂ in acetonitril (like after the synthesis: 0.05 mol l⁻¹) was dropped on a copper-grate and dried for two hours under air. Afterwards they were dried at 80 °C in the vacuum oven over night.

In Figure 12 the configuration of a TEM is shown. The virtual source at the top is an electron gun. It produces a stream of monochromatic electrons. The stream is focused to a small, thin, coherent beam by the use of the magnetic condensor lenses 1 and 2. The first lens determines the general size range of the final spot that strikes the sample. The second lens changes the size of the spot on the sample from a wide disperse spot to a pinpoint beam. The beam is restricted by the condenser aperture, knocking out high angle electrons. Next the beam strikes the sample and parts of it are transmitted. An objective lens focuses the transition portion into an image. Optional objective and selected area metal apertures can restrict the beam; the object aperture enhancing contrast by blocking high-angle diffracted electrons; the selected area aperture enables the user to examine the periodic diffraction of electrons by ordered arrangements of atoms in the sample. Through the intermediate and projector lenses the image is passed down through the column, being enlarged all the way. The image strikes the phosphor image screen and light is generated, so the user can see the image. [35]

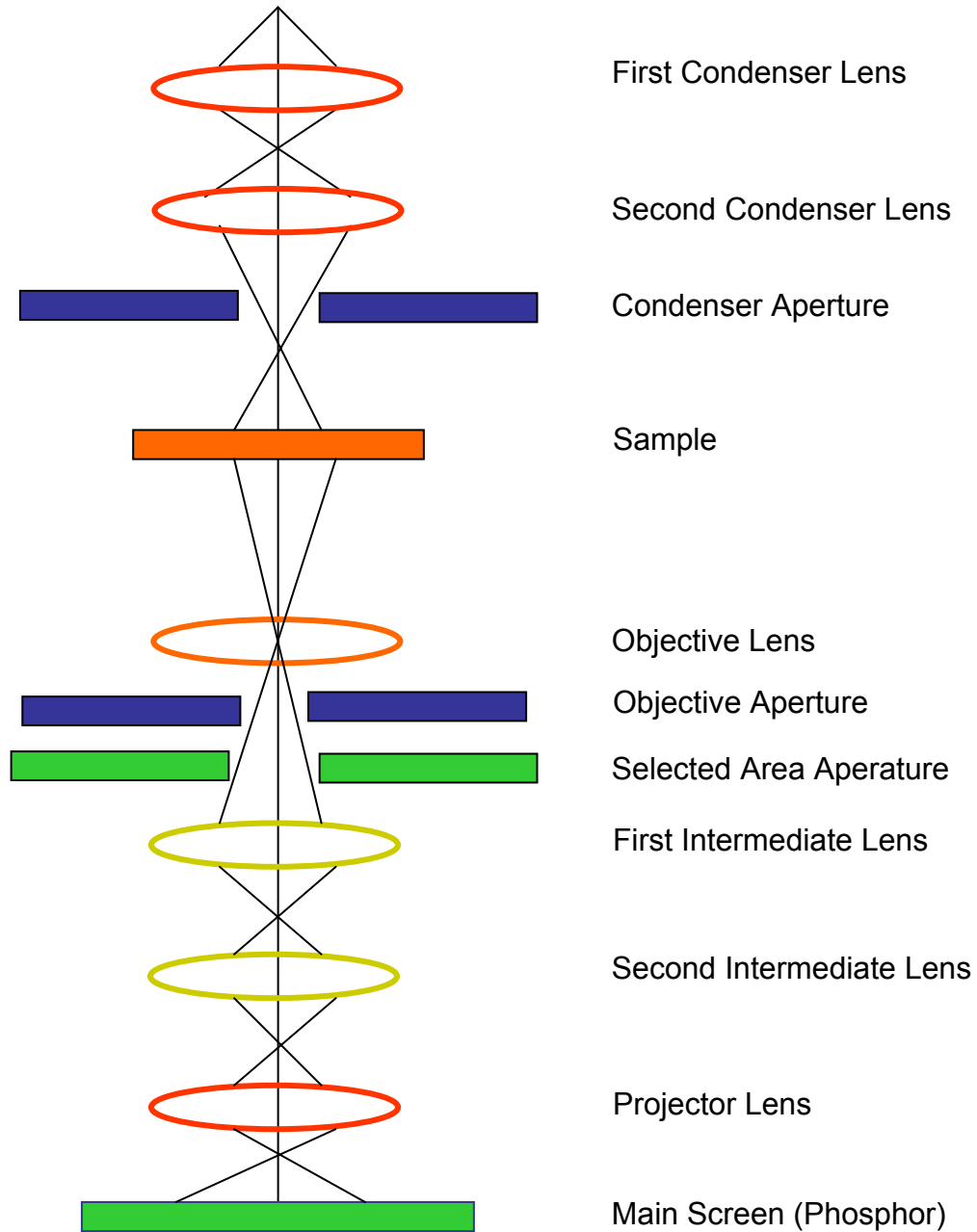


Figure 12: Configuration of a Transmission Electron Microscope

2.4 Device Preparation

For the solar cells different structures were used:

2.4.1 Solar Cell Schemata

For bilayer solar cells two different structures were used: The first structure can be seen in Figure 13. A CIS layer was spincoated on ITO covered glass, then a layer of PCBM was dropcasted and the electrodes (LiF/Al) were evaporated on top. The other structure is shown in Figure 14. A layer of CIS was spincoated on ITO covered glass and then a layer of P3HT was dropcasted on top, on this layer the Au electrodes were evaporated.

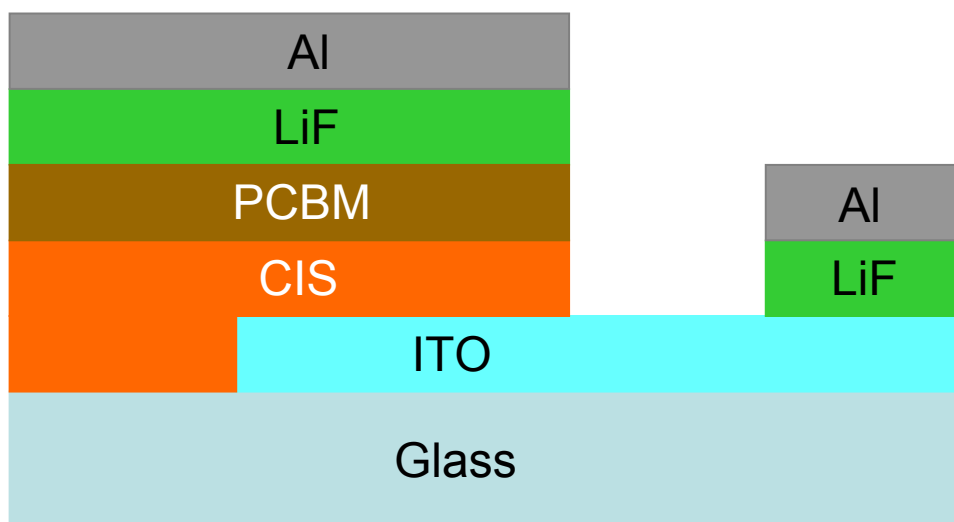


Figure 13: Scheme of a bilayer solar cell: ITO covered glass / CIS layer / dropcast PCBM layer / evaporated top electrode (LiF / Al)

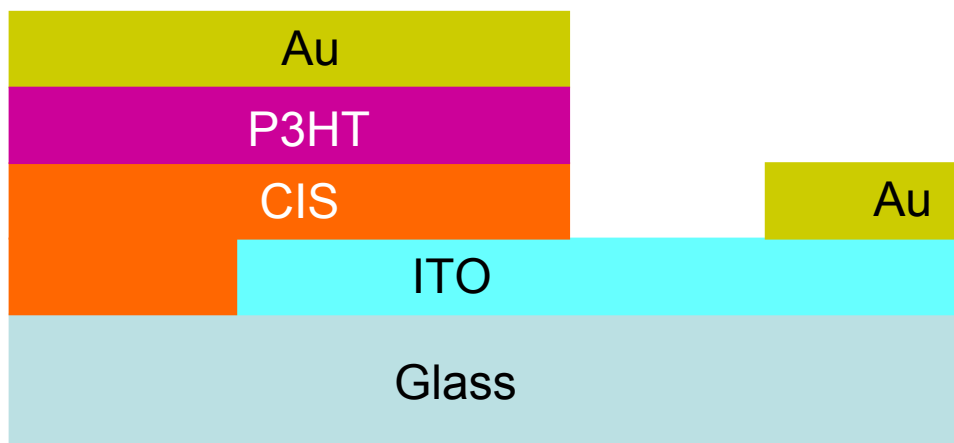


Figure 14: Scheme of a bilayer solar cell: ITO covered glass / CIS layer / dropcast P3HT / evaporated Au top electrode

The built bulk heterojunction solar cells had structures shown in Figure 15 and Figure 16. The structure in Figure 15 for bulk heterojunction cells consists of a layer of PEDOT : PSS on ITO covered glass, then a mixed P3HT and CIS layer and LiF / Al electrodes on top. In Figure 16 a mixed PCBM and CIS layer was spincoated on ITO-covered glass and LiF / Al electrodes were evaporated on top of this layer.

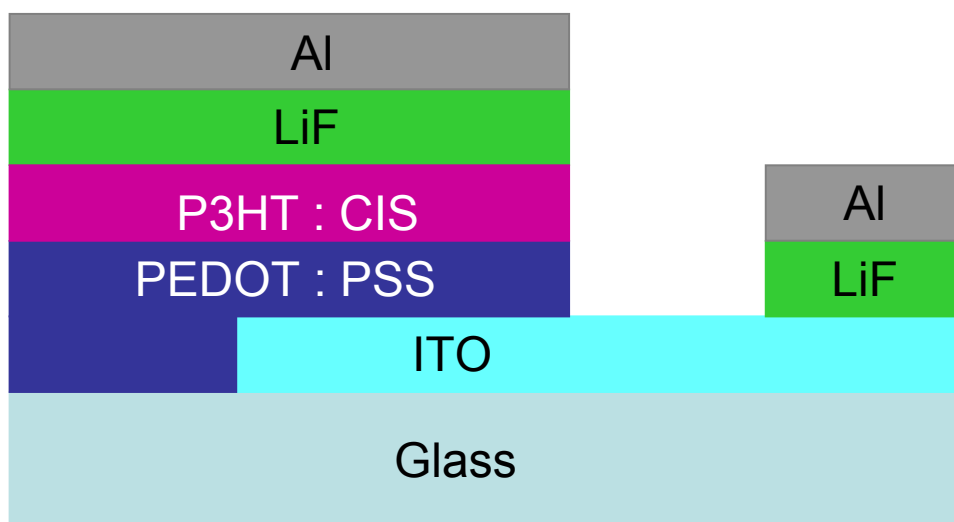


Figure 15: Scheme of a bulk heterojunction solar cell: ITO covered glass / Spincast Pedot:PSS / P3HT-CIS layer / evaporated top electrode (LiF / Al)

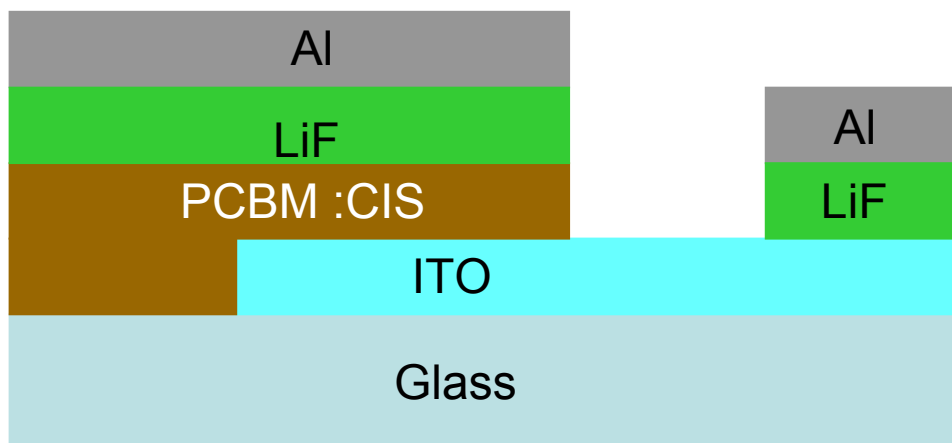


Figure 16: Scheme of a bulk heterojunction solar cell: ITO covered glass / PCBM-CIS layer / evaporated top electrode (LiF / Al)

The CISCuT-Solar cells were prepared together with Sergei Bereznev from Tallinn university of Technology (department of Material Science). They consisted of a Cu-tape with CIS bulk material on top, then was a layer of CIS nanoparticles and a semitransparent Au electrode (Figure 17)

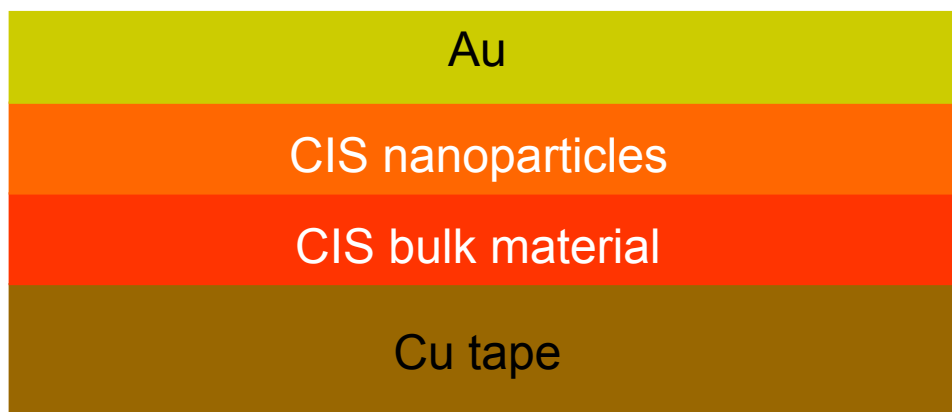


Figure 17: Scheme of a CISCuT-solar cell: Cu tape / CIS bulk material / CIS nanoparticles layer / evaporated top electrode (Au)

2.4.2 Substrate Preparation

ITO Coated Glass

Indium – tin – oxide (ITO) coated glass sheets were cut into 1.5 cm x 1.5 cm substrates for spincoating or dropcasting, and to 1.5 cm x 4.5 cm substrates for doctorblading. The ITO was purchased from Merck KgaA, Darmstadt, Germany, with an ITO thickness of 125 nm. To prevent short circuits one third of the ITO-surface was removed with strong acid ($\text{HCl}_{\text{conc.}} : \text{HNO}_3_{\text{conc.}} : \text{H}_2\text{O} = 4.6 : 0.4 : 5$). The rest of the surface was protected against the acid by a tape. After 45 minutes the acid was washed away with acetone. The substrates were now cleaned each for 15 minutes three times with acetone and once with isopropanol in an ultrasonic bath.

CIS Bulk Layer on Cu Band

These substrates were prepared by the Institut für Solare Technologie, GmbH, Frankfurt/Oder, Germany.

For cleaning, the Cu-tape was treated with phosphoric acid and electropolished in phosphoric acid. Then an indium layer was electrolytically deposited. As next step the In coated Cu tape was sulfurized. This was done in a narrow-lit reactor with multi-zone temperature control. Gaseous S_x reacted in a N₂ carrier gas flow at 700 °C with the Cu band. Then a Cu_{2-x}S layer which covers the CIS top had to be removed by a KCN etch. In the future it will be possible to perform all this processes as a roll to roll process. The Cu tape was 1 cm in width and 100 µm thick. The layer was characterized by X-ray, TEM and scanning electron microscopy. For details of the preparation of the bulk CIS layer see C. Penndorf et al. [36]. The band was cut into pieces of 1 cm x 1 cm.

The copper tape has 3 functions in this concept: It serves as mechanical carrier, as electrical bottom contact and as Cu source for the CIS layer formation.

2.4.3 CIS Layers in Bilayer Solar Cells and CISCuT - Solar Cell

These layers were used for cells as shown in Figure 13, Figure 14 and Figure 17. There were different ways to make CIS layers: one was to doctorblade with a speed of 25 mm / s a concentrated solution of CIS in pyridine or methanol on the substrate (Doctorblader, Erickson, Hemer, Deutschland). For this solution the CIS – acetonitrile solution from the synthesis was mixed 1 : 1 with the pyridine or methanol. Over night the particles precipitated and were washed with the solvent again, afterwards a part of the solvent was removed to get the concentrated solution.

The other possibility was to spincoat a solution of CIS in acetonitrile (as it is after the synthesis: 0.05 mol / l) on the substrate. The spincoating was done 2 times in the Ar – glovebox (M. Braun, Gerching, Germany) with a spincoater P 6700 from Specialty Coating Systems, Inc. , Indianapolis, USA with a speed of 700 rpm for 40 s.

Afterwards the samples were dried on a heatplate in the glovebox at elevated temperatures.

For the CISCuT cells the nanoparticles were spincoated two times (700 rpm / 40 s) on the Cu tape substrate. Afterwards they were annealed at 200 °C on the hot plate in the glove box over night.

2.4.4 PCBM Layer in Bilayer Solar Cells

The systematic name of PCBM is 1 - (3 - methoxycarbonyl) propyl – 1 - phenyl [6,6]C₆₁. It is a derivate of a Buckminsterfullerene and the side chain changes the properties. Therefore PCBM is soluble in organic solvents like chlorobenzene or toluene. The chemical structure of PCBM can be seen in Figure 18. The used PCBM was purchased from Nano-C, Boston, USA. It was used as electron-acceptor.

PCBM was dropcast (40 µl / cell) or spincoated (1500 rpm, 40 s) from 3 wt % solutions in chlorbenzene. The devices were dried under vacuum for 45 minutes.

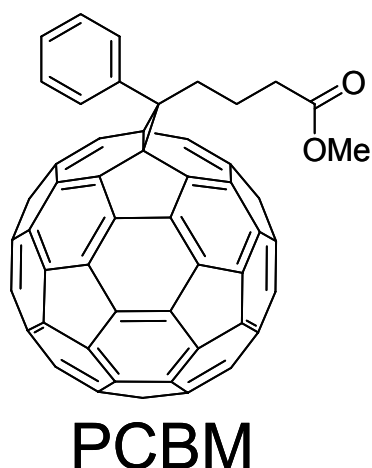


Figure 18: Chemical Structure of PCBM

2.4.5 P3HT Layers in Bilayer Solar Cells

The systematic name of P3HT is Poly(3 - hexylthiophene - 2,2 - diyl). For this thesis regioregular P3HT from Rieke Metals, Inc., Lincoln, USA was used. The chemical structure can be seen in Figure 19. It is highly soluble in common organic solvents.

P3HT was spincoated (1500 rpm, 40 s) or dropcast (40 μ l / cell) from 1 wt % solutions in chlorobenzene or chloroform. The devices were dried under vacuum for 45 minutes.

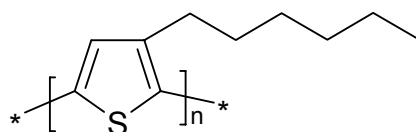


Figure 19: Chemical Structure of P3HT

2.4.6 PEDOT:PSS Layers

PEDOT:PSS layers were used for cells with a geometry as shown in Figure 15. PEDOT:PSS is a mixture of poly(3, 4 - ethylenedioxythiophene) and poly(styrenesulfonate). It was purchased from Bayer AG, Leverkusen, Germany. The aqueous dispersion (particle size of 80 nm, 0.5 w% PEDOT:PSS = 2 : 3) was spincoated twice on the ITO substrate (1500 rpm, 40 s) and dried over night under vacuum. PEDOT : PSS is used as an interfacial hole conducting and electron blocking layer.

Figure 20 shows the chemical structure:

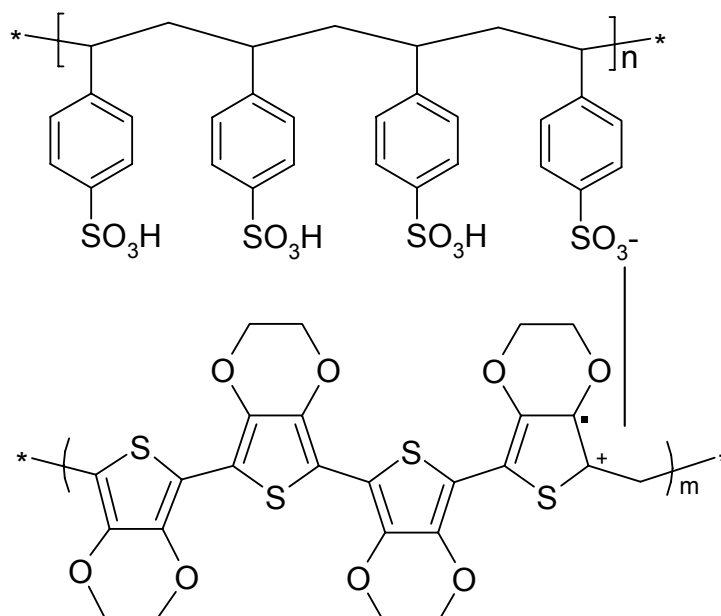


Figure 20: Chemical structure of electrochemical doped PEDOT:PSS

2.4.7 Mixed Layers of CIS and PCBM or P3HT in Bulk Heterojunction Cells

CIS was precipitated and washed just as explained in 2.4.3. Then the particles were kept in the vacuum oven over night at 80 °C. From now on the work was done in the glovebox. The dried particles were mixed with either the 3 wt % PCBM solutions in chlorobenzene or the 1 w % P3HT solutions in chlorobenzene in different weight-ratios. The dispersions were stirred over night. Then they were spincoated (1500 rpm, 40s) or dropcasted (40 µl / cell) on the substrate. The devices were dried on the heatplate at 60 °C for 2 h. These layers were used for cells with a geometry shown in Figure 15, and Figure 16.

2.4.8 Top Contact Evaporation

After the active layers were applied the top contacts were thermally evaporated under high vacuum (approximately $1 \cdot 10^{-5}$ mbar) in a Leybold evaporation chamber (Leybold Vacuum, Cologne, Germany). The metals for the evaporation were placed into a tungsten boat. The evaporation rate (0.005 nm / s for LiF, 0.01 increasing to 0.1 nm / s for Al and 0.1 nm / s for Au) was monitored by a quartz balance, Intellemetrics IC 600. The evaporation was done through a shadow mask. 0.6 nm of LiF were followed by 80 nm of Al. The interfacial layer of LiF is known to improve the electron exitation, respectively injection [37] and also an increase in fill factors and a stabilization of high V_{oc} 's are observed [38]. For the cells with Au as top contact 80 nm were evaporated except for the CISCuT-cells: only 5 nm of Au were evaporated because the contact has to be semitransparent.

2.5 AFM Measurements

Atomic force microscope (AFM) measurements were done with a Dimension 3100 instrument from Digital Instruments (Santa Barbara, CA) in tapping mode. AFM pictures were applied to check the roughness of the films: this was used to see the distribution of the materials in bulk heterojunction cells, to estimate the size of the CIS-particles and to see if the material makes a real film or if there are just islands of the material within the device.

2.6 Current-Voltage Measurements

These measurements were done in an Ar-glovebox. A Streunagel solar simulator (K. H. Streunagel Lichttechnik GmbH, Mörfelden-Walldorf, Germany, with metal halogen lamp as light source and with an AM 1.5 filter) was used. For the measurements the intensity was calibrated to 100 mW cm⁻². The $J - V$ curves were measured with a Keithley 236 (Keithley Instruments, Inc. , Cleveland, Ohio; USA) sweeping from $- 2.5$ V to $+ 2.5$ V. The electrodes were ITO and LiF/Al or Au.

$J - V$ curves give important parameters to describe a solar cell. These parameters are: The open-circuit voltage (V_{OC}), the short-circuit current (j_{SC}) and the maximum-power-point (mpp). The mpp is defined as the point inside the fourth quadrant where the product of J times V has a maximum. It defines the maximum-power voltage (V_{mpp}) and the maximum-power current (j_{mpp}). This can be seen in Figure 21.

Another important parameter for solar cells is the fill factor (FF). It describes the quality of the diode:

Equation 2

$$FF = \frac{V_{mpp} * j_{mpp}}{V_{OC} * j_{SC}}$$

For an ideal diode FF approaches 1. With the FF the efficiency can be calculated

Equation 3

$$\eta_{AM1.5} = \frac{j_{SC} * V_{OC} * FF}{P_{light}}$$

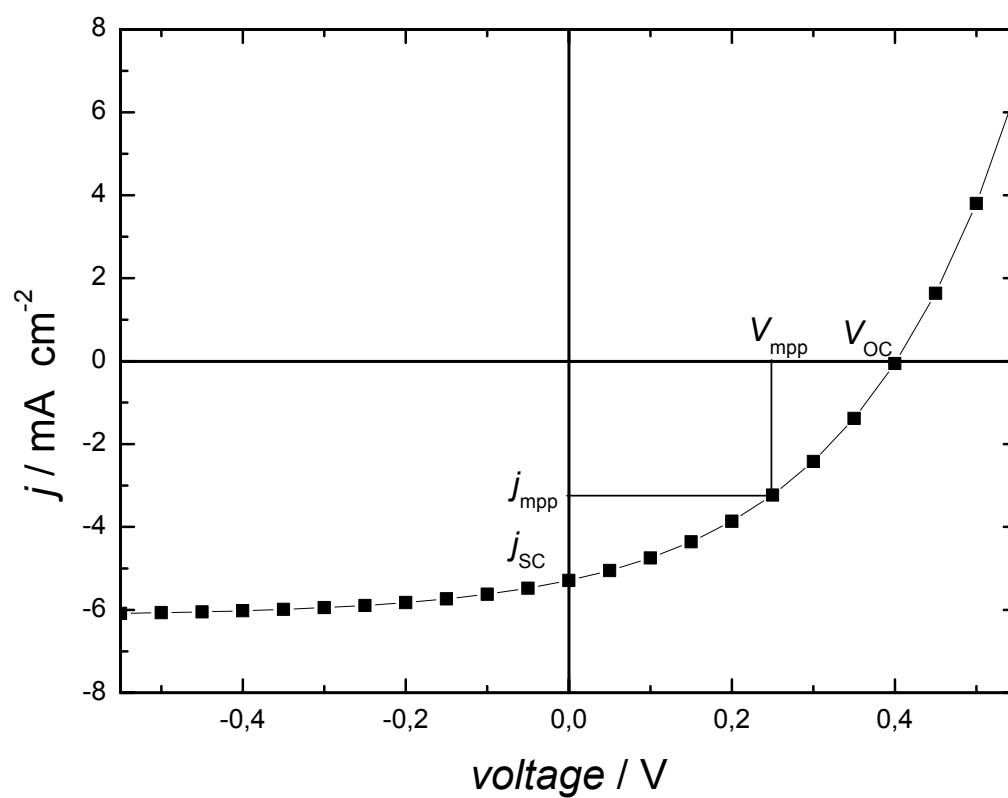


Figure 21: Definition of V_{OC} , j_{sc} , V_{mpp} , j_{mpp}

2.7 IPCE Measurements

The incident-photon-to-current-efficiency (IPCE) or incident-photon-to-collected-electron-efficiency, gives the spectral resolution of the photocurrent.

The measurements were done with a home made setup in the Ar-glovebox. The light from a 80 W Xe-lamp (Müller Elektronik Optik LXH100, Moosinning, Germany) was optically chopped (Scitec Instruments Ltd. 300C, Cornwall, UK) with 73 Hz. With a light fiber the monochromatized light (monochromator by Acton Research Corp. FA448M, Acton, USA) was focused on the sample. The lamp spectra was calibrated with a monocrystalline silicone diode with a known sensitivity (Melles Griot, Carlsbas, USA). A lock-in amplifier (EG&G Instruments 7260, Gaithersburg, USA) was used. The IPCE can be calculated with Equation 4:

Equation 4:
$$IPCE = 1240 * \frac{j}{\lambda * P_{in}} * 100$$

Units:

$IPCE \dots \dots \%$	$1240 \dots V \text{ nm}$	$j \dots \dots \mu A \text{ cm}^{-2}$
$\lambda \dots \dots \text{nm}$	$P_{in} \dots \dots W \text{ m}^{-2}$	

P_{in} is the light power incident on the device.

3 Results and Discussion

3.1 Changes in the Synthesis

Five different syntheses were done during this thesis: June, 6th 2004 (batch1), September, 9th 2004 (batch 2), November, 1st 2004 (batch 3), January, 18th 2005 (batch 4) and May, 16th 2005 (batch 5).

In this synthesis 3 things were varied: the amount of Bis(trimethylsilyl)sulphide, the amount of TPP and the second step was done once under N₂-atmosphere instead of Ar-atmosphere.

In batch 1 Bis(trimethylsilyl)sulphide was added in a stoichiometric ratio of Cu : In : S = 1 : 1 : 2.2 (9.4 ml), TPP was added in the first step of the synthesis (10 ml per reaction flask) and in the second step of the synthesis (10 ml together with the Bis(trimethylsilyl)sulphide), all steps were done in Ar-atmosphere.

In batch 2 and 3 Bis(trimethylsilyl)sulphide was added in a stoichiometric ration of Cu : In : S = 1 : 1 : 2 (8.4 ml), TPP was added in the first step of the synthesis (10 ml per reaction flask) and in the second step of the synthesis (10 ml together with Bis(trimethylsilyl)sulphide), all steps were done in Ar-atmosphere.

In batch 4 Bis(trimethylsilyl)sulphide was added in a stoichiometric ratio of Cu : In : S = 1 : 1 : 2 (8.4 ml), TPP was added in the first step of the synthesis (10 ml per reaction flask), all steps were done in Ar-atmosphere. In the second step of the reaction no TPP was used (the Bis(trimethylsilyl)sulphide was only mixed with acetonitrile for dilution), to reduce the amount of TPP in the end product due to the bad influence of TPP on the film forming properties.

In batch 5 the ratio was 1 : 1 : 2.3 (9.7 ml), Bis(trimethylsilyl)sulphide was added in the first and in the second step (as in batch 1, 2, 3) and the second step of the reaction was done in N₂-atmosphere.

As it will be shown, the particles of batch 1 worked best in combination with P3HT, the particles of batch 2, 3 and 4 worked best in combination with PCBM and the particles of batch 5 could not be used for making a solar cell.

Another difference was that the particles of batch 1, 2 and 3 could be precipitated by adding methanol (1 : 1) to the acetonitrile solution and the particles of batch 4

and 5 could not. It was always possible to precipitate the particles by adding pyridine (1 : 1) to the acetonitrile solution.

3.2 X- Ray Spectroscopy

The crystallographic structure of the particles were determined by powder X-ray diffraction. The powder was gained by precipitating the particles with methanol or pyridine and drying them in the vacuum oven.

Figure 22 shows the X-ray diffraction pattern of CIS powder of 3 batches. As one can see the location of the pattern is in good agreement with the Joint Committee on Powder Diffraction Standards (JCPDS) reference diagram (card 27-0159) for the corresponding bulk phases [5]. An intense peak at $2\theta = 27.9^\circ$ oriented along the (112) direction and other prominent peaks observed at 46.5° ((220)/(204)) and 55.0° ((312)/(116)) indicate the chalcopyrite structure of CIS.

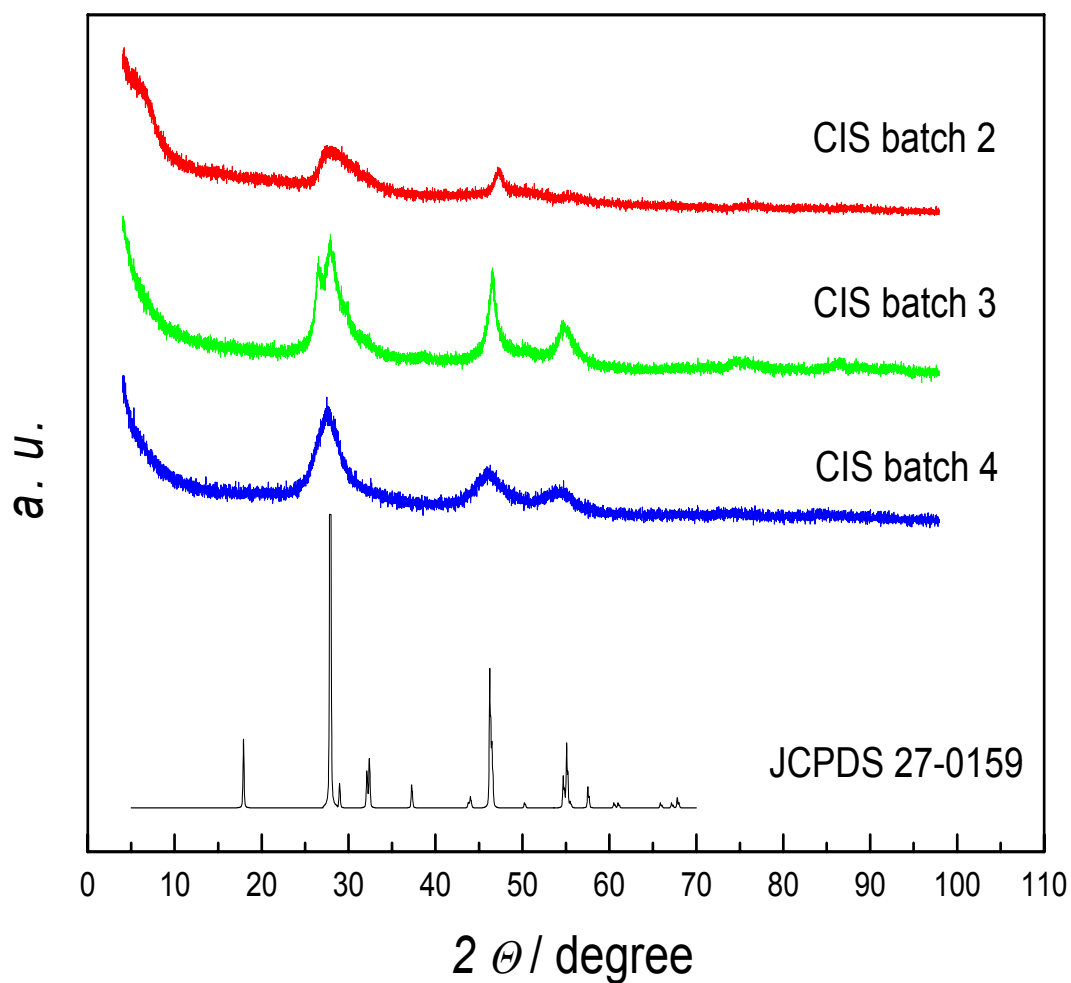


Figure 22: X-ray diffraction pattern of CIS nanocrystals in comparison with a reference diagram for CIS in the bulk phase from JCPDS

Figure 23 shows that the starting products CuI and InCl₃ are not visible inside the endproduct.

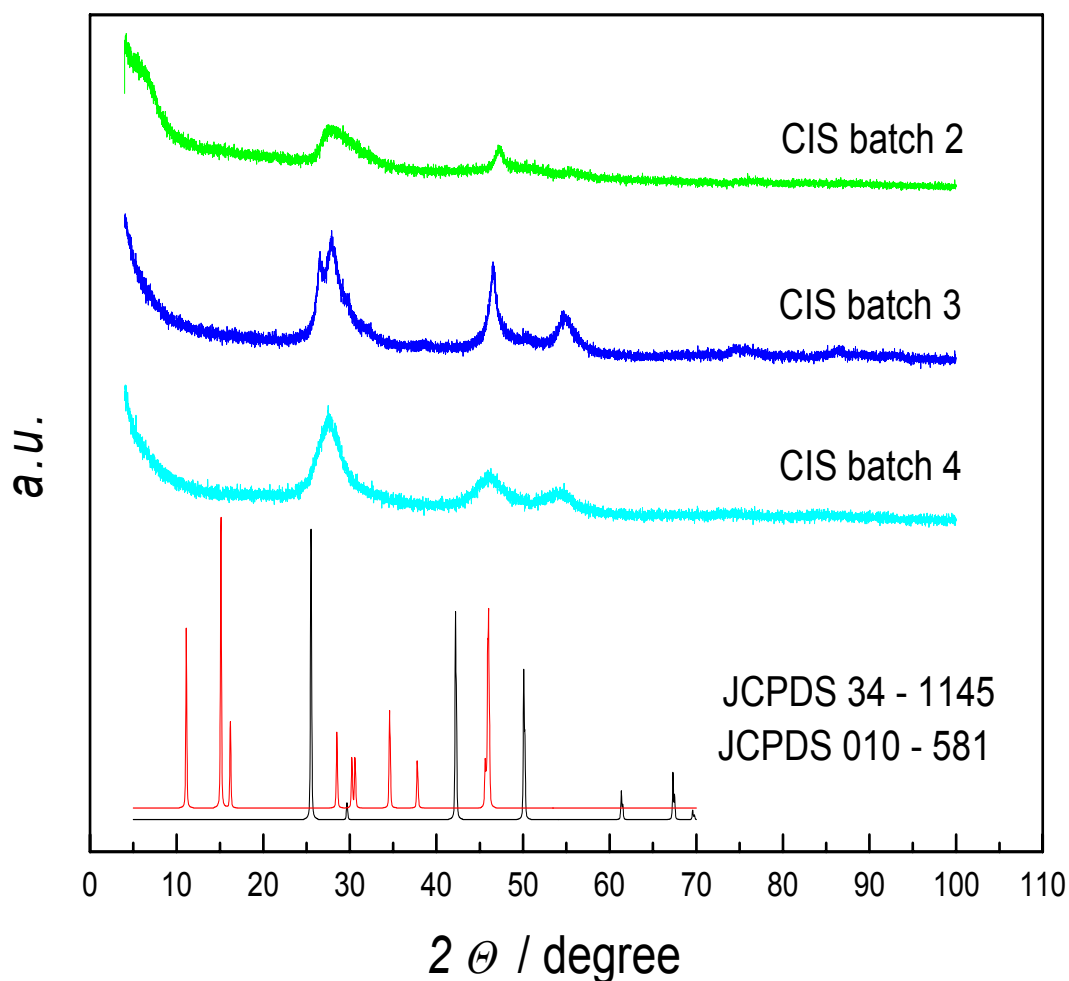


Figure 23: X-ray diffraction pattern of CIS nanocrystals in comparison with a reference diagrams for CuI and InCl₃ from JCPDS

It is important to mention that the intensities of the samples are much lower than the intensities of the references. The low intensities can be explained by two facts: First the reference is of CIS in the bulk phase and the sample was measured from powder, which has lower intensities. Second the intensity depends on the measuring speed: whereas the samples in this thesis were measured at normal speed, samples used as reference are measured at lower speeds to gain higher intensities.

3.3 TEM

High-resolution transmission electron microscope images were done from the particles of batch 2 and 3. As Figure 24 and Figure 26 show a broad distribution of the particle sizes is revealed. Size distribution of CIS was found in the range from 20 nm to 500 nm. The electron diffraction pattern displayed in Figure 25 and Figure 27 shows the presence of polycrystalline nanostructures with characteristic broad reflection spots and also very sharp spots of reflection, indicating the existence of larger particles. Also in Figure 27 an amorphous region is shown.

This results do not correlate to the AFM-pictures that will be shown in 3.4. The resolution of the TEM images is limited due to statistic distribution of the CIS clusters in the sample. Even if the amount of large crystals are less, they dominate the TEM image. Therefore, the TEM investigation always leads to an overestimation of the average size. [12] Also the preparation of the particles on the copper grate can change the size distribution. It is possible that the particles agglomerate to bigger particles while drying in the vacuum oven.

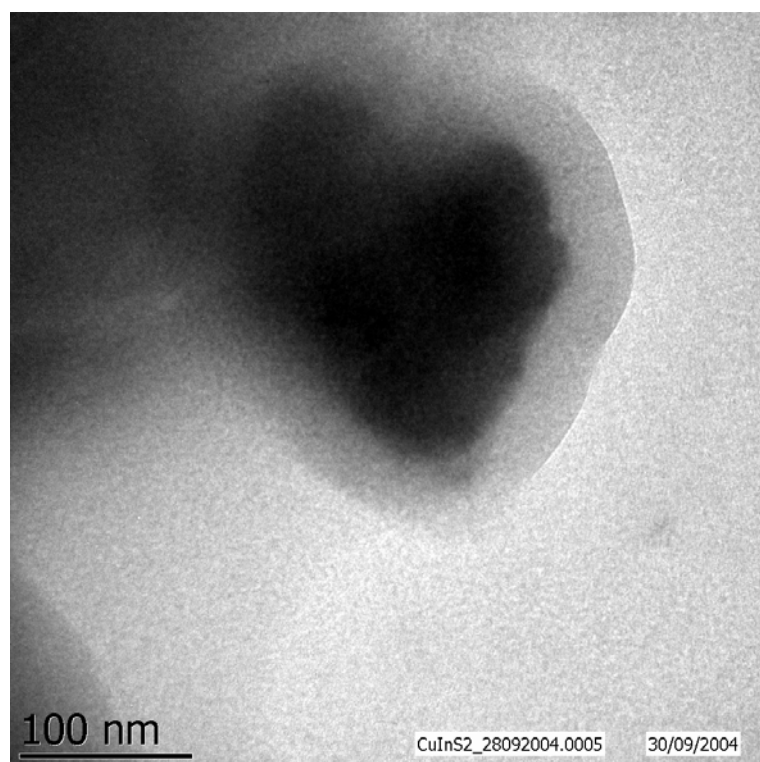


Figure 24: HRTEM image of TPP-protected CIS-particles (batch 2)

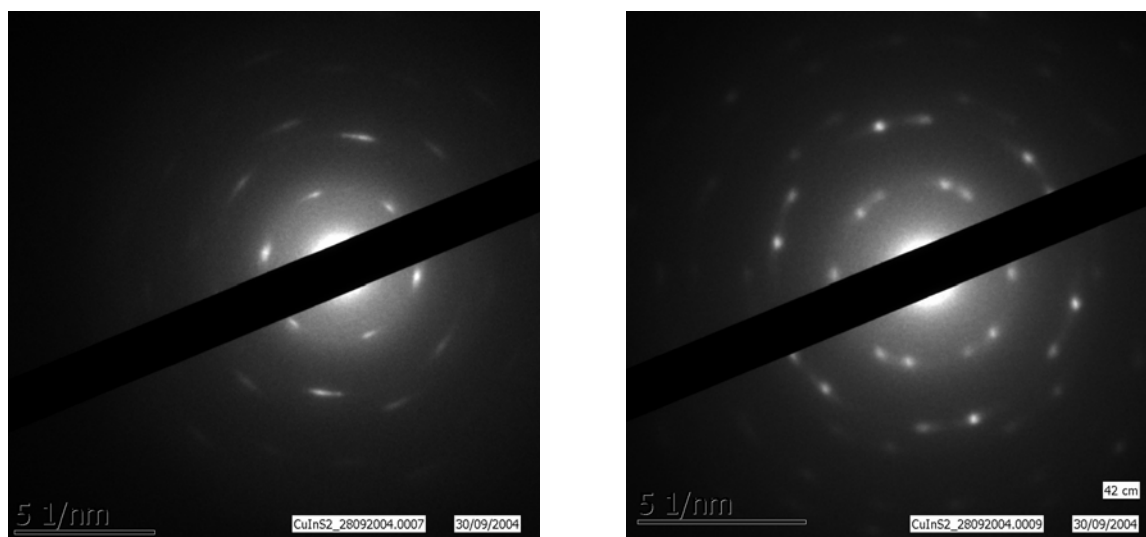


Figure 25: Selected-area electron diffraction pattern of TPP-protected CIS-particles (batch 2)

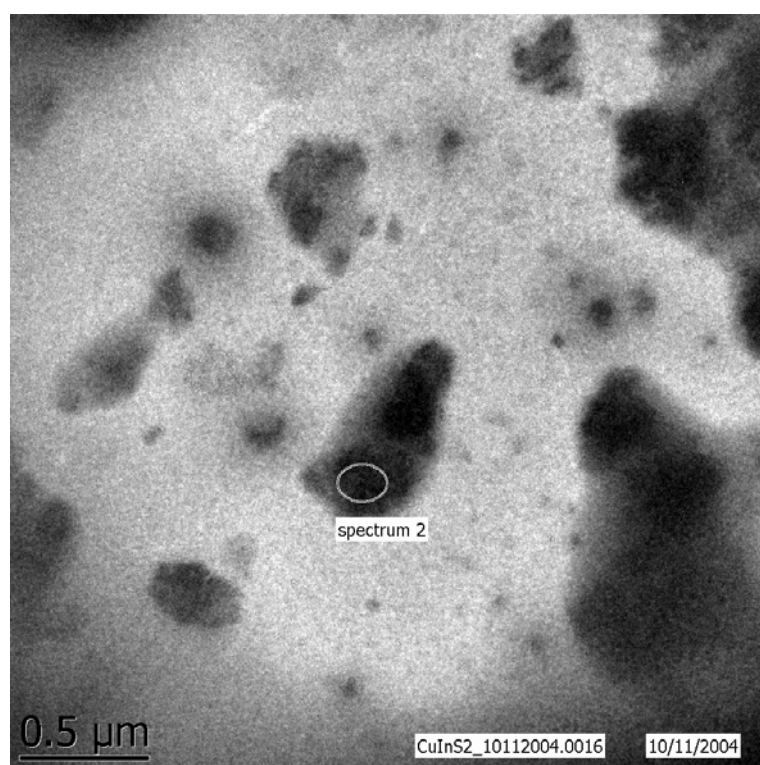


Figure 26: HRTEM image of TPP-protected CIS-particles (batch 3)

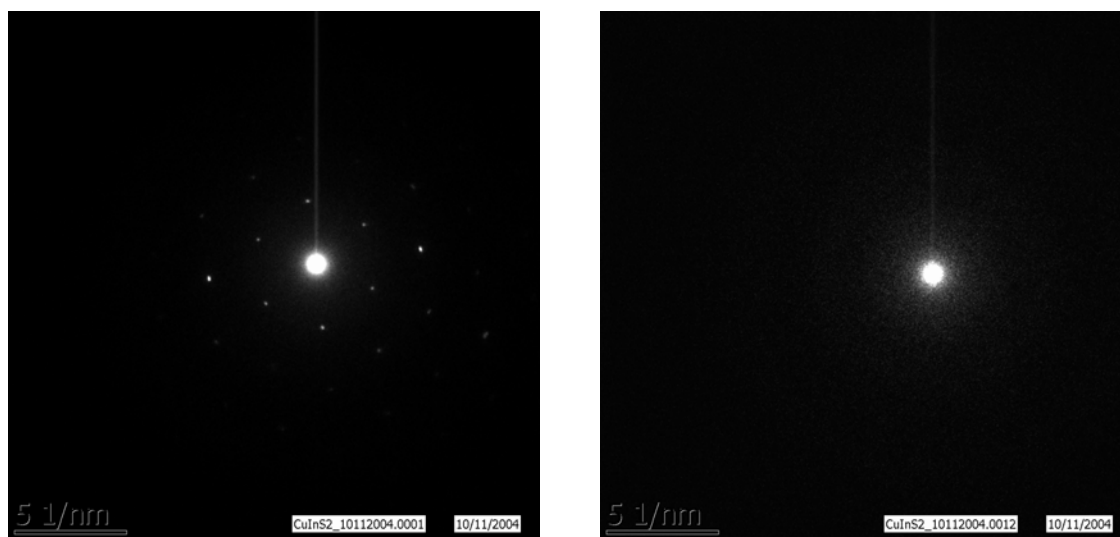


Figure 27: Selected-area electron diffraction pattern of TPP-protected CIS-particles (batch 3)

It is important to mention that the EDX elemental analysis could not be used. The amount of copper could not be calculated in a proper way because the peaks for copper also indicate the copper grate and not only the copper in the particles.

3.4 AFM Measurements

3.4.1 Substrates and PEDOT:PSS

AFM pictures of cleaned ITO-glass and PEDOT-PSS spincoated on cleaned ITO-glass were taken.

The ITO substrates (Figure 28) have a roughness of 20 nm.

Figure 29 shows CIS in the bulk phase on Cu band. This substrates were used for the CISCuT solar cells. As can be seen the surface is very rough.

The PEDOT:PSS layer (Figure 30) on ITO has only a roughness of 15 nm, that means it is flattening the surface of ITO.

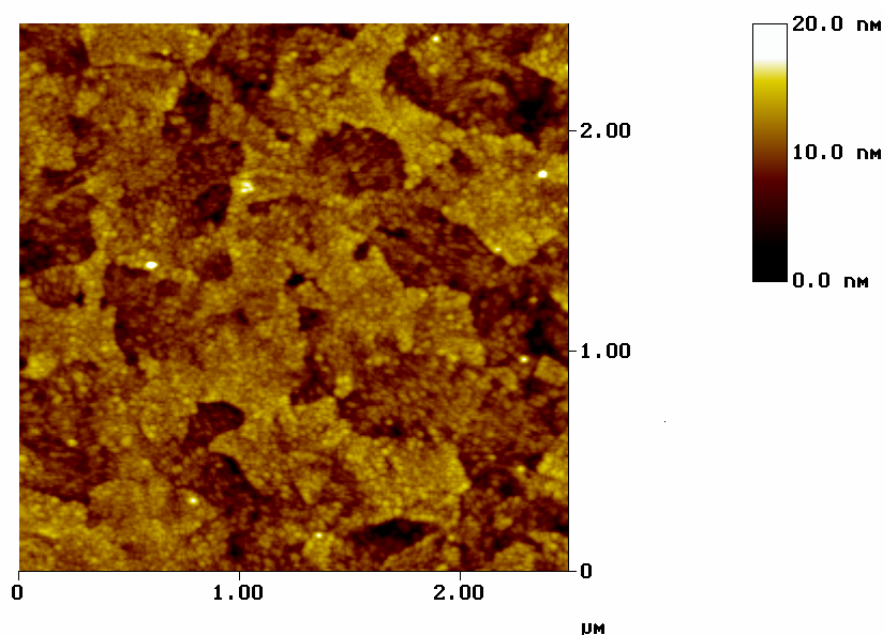


Figure 28: AFM picture of the ITO substrate.

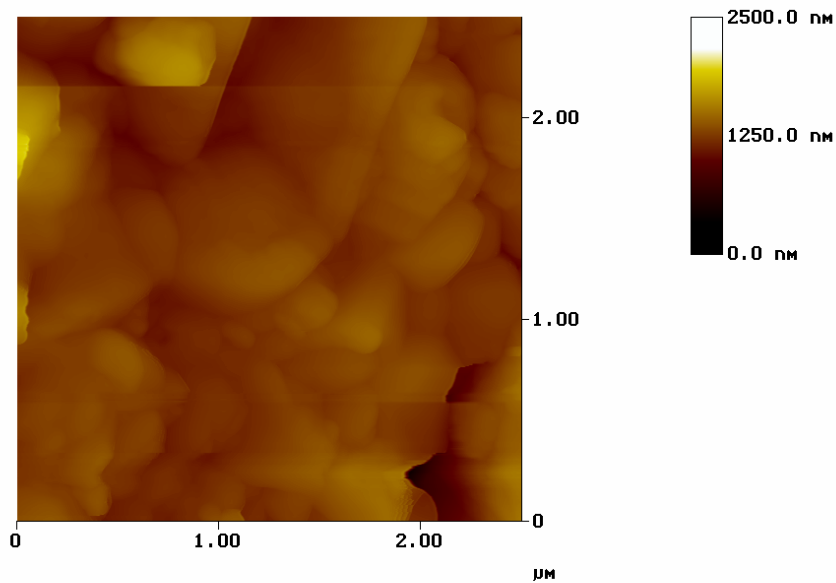


Figure 29: AFM image of the bulk CIS on a Cu band for CISCuT solar cells

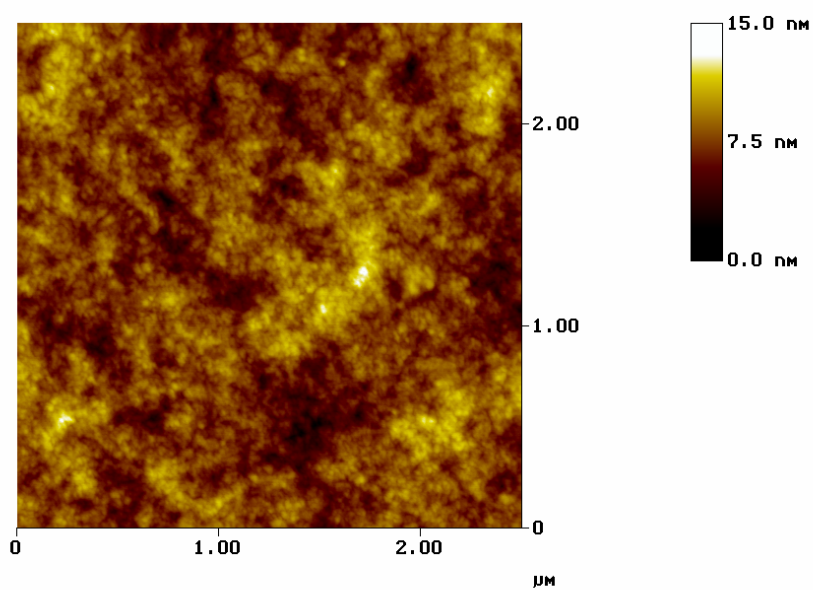


Figure 30: AFM picture of spincoated a Pedot:PSS film on ITO glass

3.4.2 Single Layers of PCBM, P3HT and CIS

AFM pictures of the single layers of CIS, PCBM and P3HT on clean ITO-glass were taken.

The P3HT was spincoated from a 1 wt % solution in chlorobenzene. The roughness of the film (Figure 31) is about 20 nm.

The CIS-layer was dropcast from a 0.05 mol l⁻¹ acetonitrile solution. The roughness of the film is about 45 nm and shows clusters of a size between 30 and 70 nm (Figure 32). This indicates, that the particles are about this size.

The PCBM layer was spincoated from a 1 wt % solution in chlorobenzene. The roughness of the film (Figure 33) is about 5 nm.

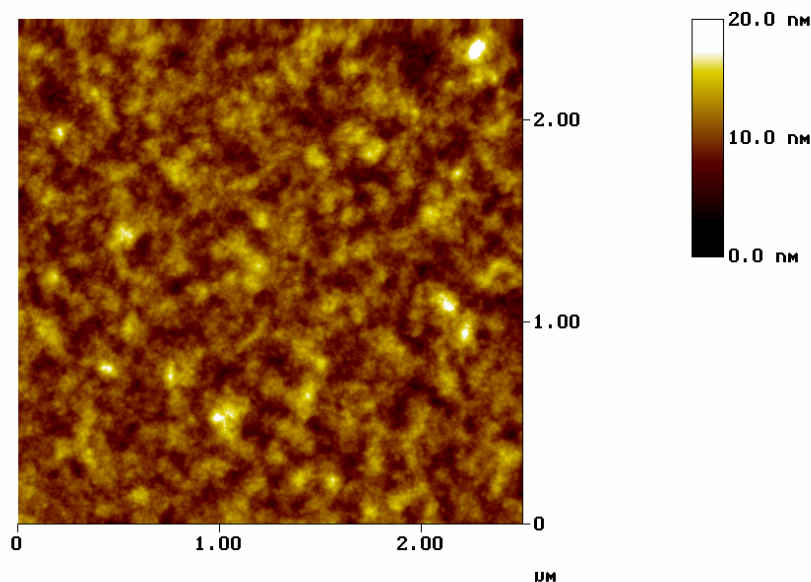


Figure 31: AFM picture of a spincoated P3HT film on ITO glass

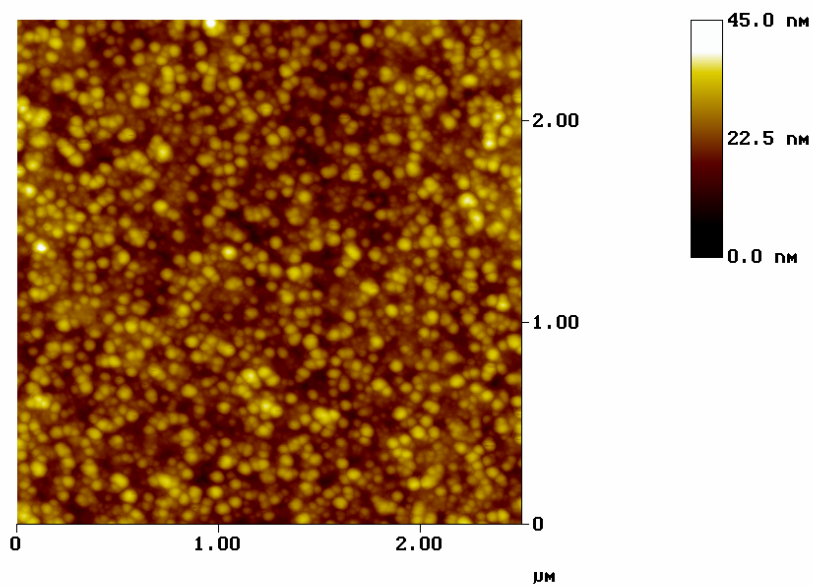


Figure 32: AFM picture of dropcast CIS-particles from a acetonitril-solution on ITO glass

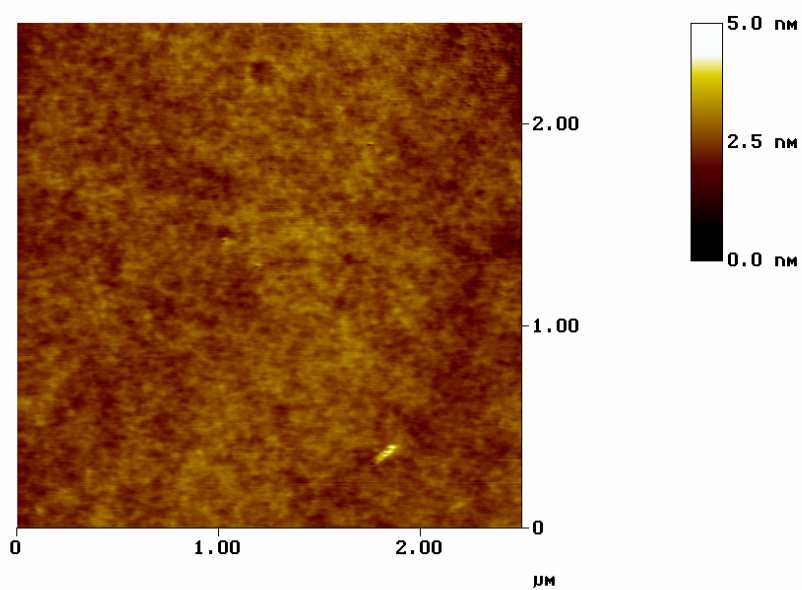


Figure 33: AFM picture of a PCBM film spincoated on ITO glass

3.4.3 Bulk Heterojunction Solar Cells

Figure 34 shows the AFM-image of a CIS-PCBM bulk heterojunction solar cell. If one compares the picture with Figure 33 it is obvious that figure Figure 34 also shows only PCBM. Therefore an optical surface image was taken (Figure 35). It shows a very high roughness of the layer. It can be assumed that the nanoparticles aggregated to very big clusters and that the layer is highly phase separated.

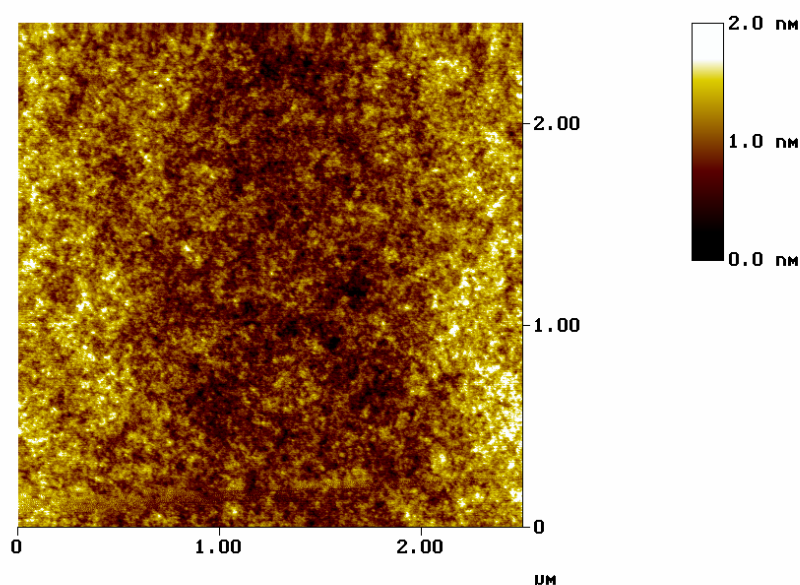


Figure 34: AFM-picture of a PCBM:CIS bulk heterojunction solar cell on ITO glass

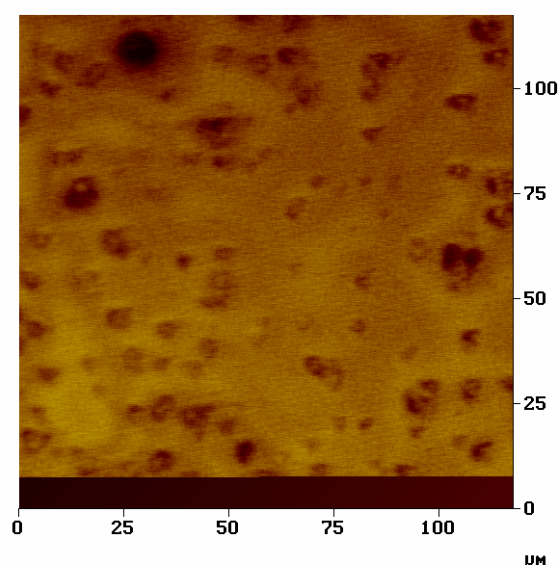


Figure 35: Optical image of a PCBM:CIS bulk heterojunction solar cell on ITO glass.

The P3HT:CIS bulk heterojunction solar cell (Figure 36) shows a roughness of 80 nm. The surface is very inhomogeneous, there are some spikes with the height of 80 nm and a diameter of 250 nm while other regions are of lower height.

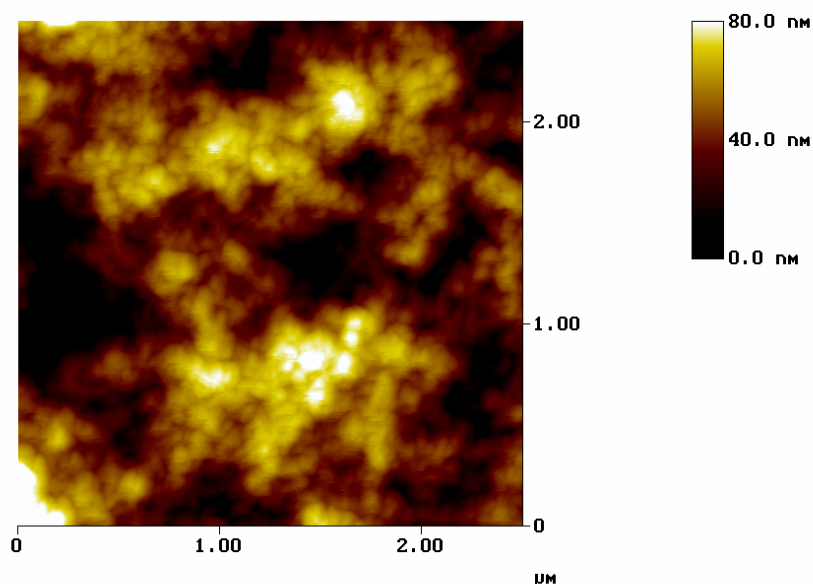


Figure 36: AFM-picture of a P3HT:CIS bulk heterojunction solar cell on top of a layer of PEDOT:PSS on ITO glass

3.4.4 Bilayer Solar Cells

In Figure 37 and Figure 38 images of CIS : PCBM solar cells are shown. These cells were prepared in exactly the same way but it is obvious that the structure of the layers is very different. Figure 37 shows a very homogenous surface with a roughness of 7 nm and only very few clusters with a diameter of around 100 nm. Figure 38 shows a surface with lots of clusters with diameters up to 400 nm and a roughness of 15 nm. This different surface also shows different behaviours of solar cells as will be shown in 3.5. Both pictures show that the layer of PCBM smoothens the surface because the roughness of the CIS-layer as shown in Figure 32 is around 45 nm.

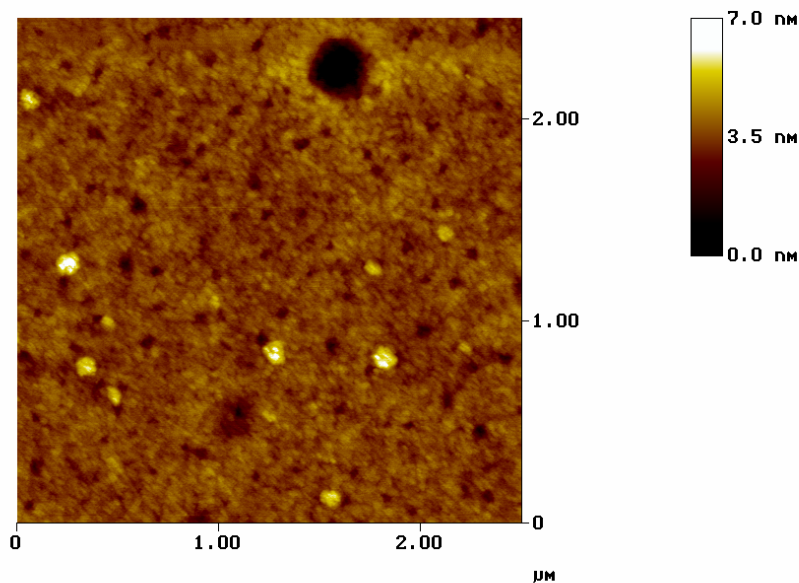


Figure 37: AFM picture of a CIS / PCBM bilayer solar cell on ITO glass without clusters

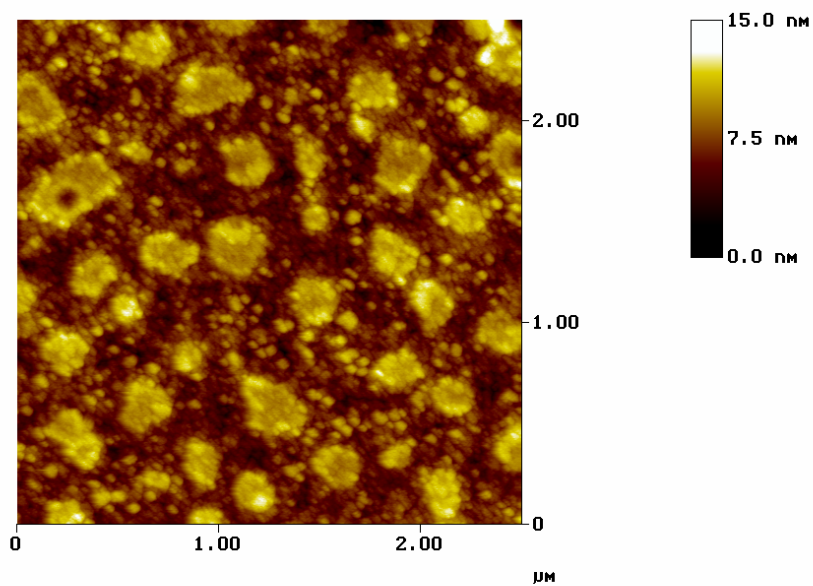


Figure 38: AFM picture of a CIS / PCBM bilayer solar cell on ITO glass with clusters

Figure 39 shows the image of a CIS / P3HT solar cell. The surface roughness is 75 nm and the surface looks homogeneous.

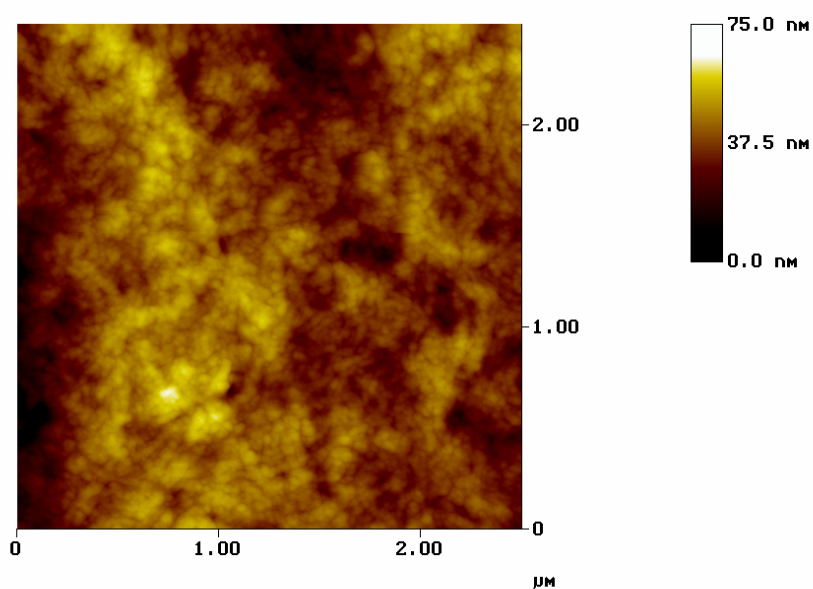


Figure 39: AFM picture of a CIS : P3HT bilayer solar cell on ITO glass

3.5 Examples for Solar Cells

The dark curves were measured to check if the device shows a diode characteristic or is short circuited. Therefore the rectification ratio was calculated too. The rectification ratio (RR) is defined as the absolute value of forward current (at a certain positive voltage) divided by the absolute value of the backward current (at the corresponding negative voltage).

Afterwards the curves under illumination were measured to get the solar cell key data (V_{OC} , j_{SC} , FF , $\eta_{AM1.5}$)

3.5.1 Bilayer Solar Cells

It is important to mention that the bilayer cells in this thesis are not bilayer cells in a strict point of view. The CIS layer is partly soluble in the solvents (chlorobenzene, chloroform) that are used for the PCBM and P3HT layers. Therefore while dropcasting parts of the CIS layer will dissolve in the other solution and built a mixed layer, this can be called a diffuse bilayer heterojunction cell [16].

CIS/PCBM

For these cells no PEDOT:PSS was used due to the ability of PEDOT:PSS as donor. It was important to be sure that only CIS reacts as donor and not PEDOT:PSS. Also at the higher temperatures which were used for the drying process of the CIS PEDOT:PSS may not be stable.

These cells were made with CIS particles from batch 3 and 4.

In different experiments different temperatures and times for the drying of the CIS layers were used. It was found that only temperatures over 100 °C and times longer than 12 h could be used. If lower temperatures or shorter times were used the samples were not dry and could not be used for further proceeding. Therefore all the samples were dried at 120°C over night.

The cells were all produced in the same way although the solar cell key data (V_{OC} , j_{SC} , FF , *rectification ratio*, ...) were very different and not reproducible.

Figure 40 shows the $J - V$ characteristics of one of the better samples: the V_{OC} is 500 mV, the short circuit current is 0.3 mA cm^{-2} , the fill factor is 0.3, and the efficiency is 0.04%

An AFM picture of this sample was shown above in Figure 38. Figure 37 shows the AFM picture of another sample. Even though the sample in Figure 37 shows the lower roughness, the key data are worse. This may be due to the small pinholes, seen in Figure 37.

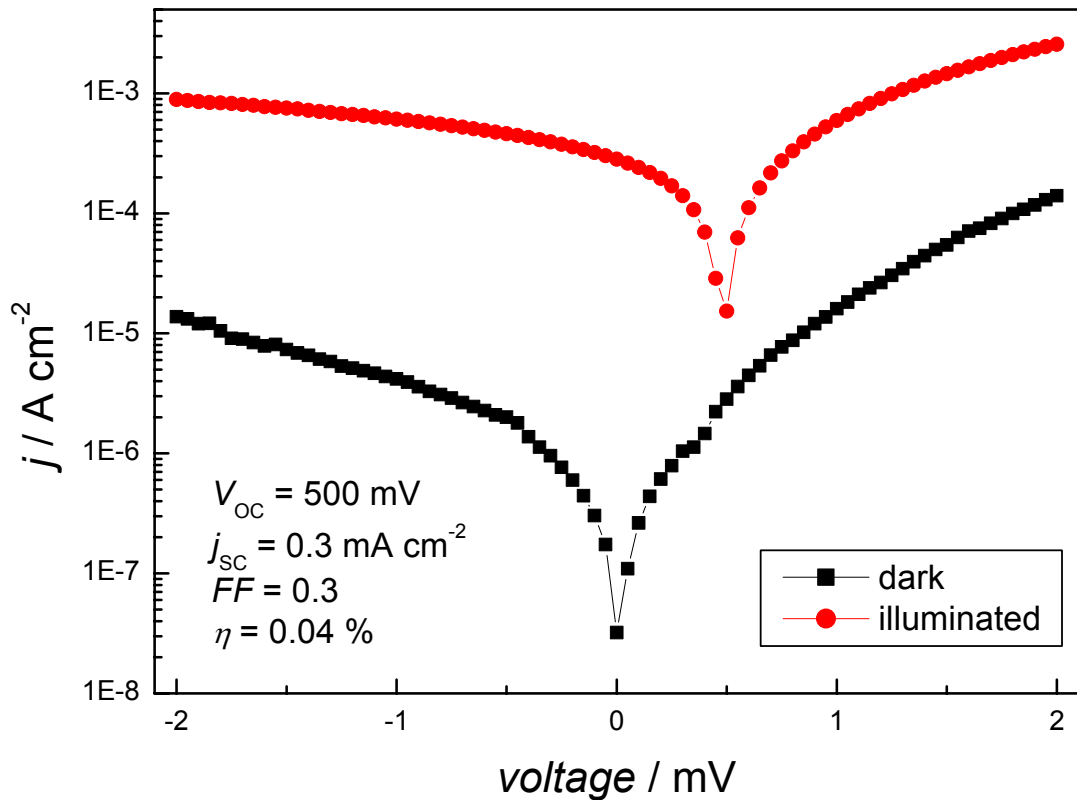


Figure 40: $J - V$ characteristic in logarithmic plot of a CIS/PCBM bilayer solar cell on ITO glass

CIS /P3HT

These cells were produced by using the particles from batch 5. The CIS films were dried at 120 °C over night. In Figure 41 a $J - V$ characteristic of a CIS / P3HT bilayer cell is shown. Under illumination no V_{OC} and j_{SC} could be measured, even if it shows a rectification ratio of 13.

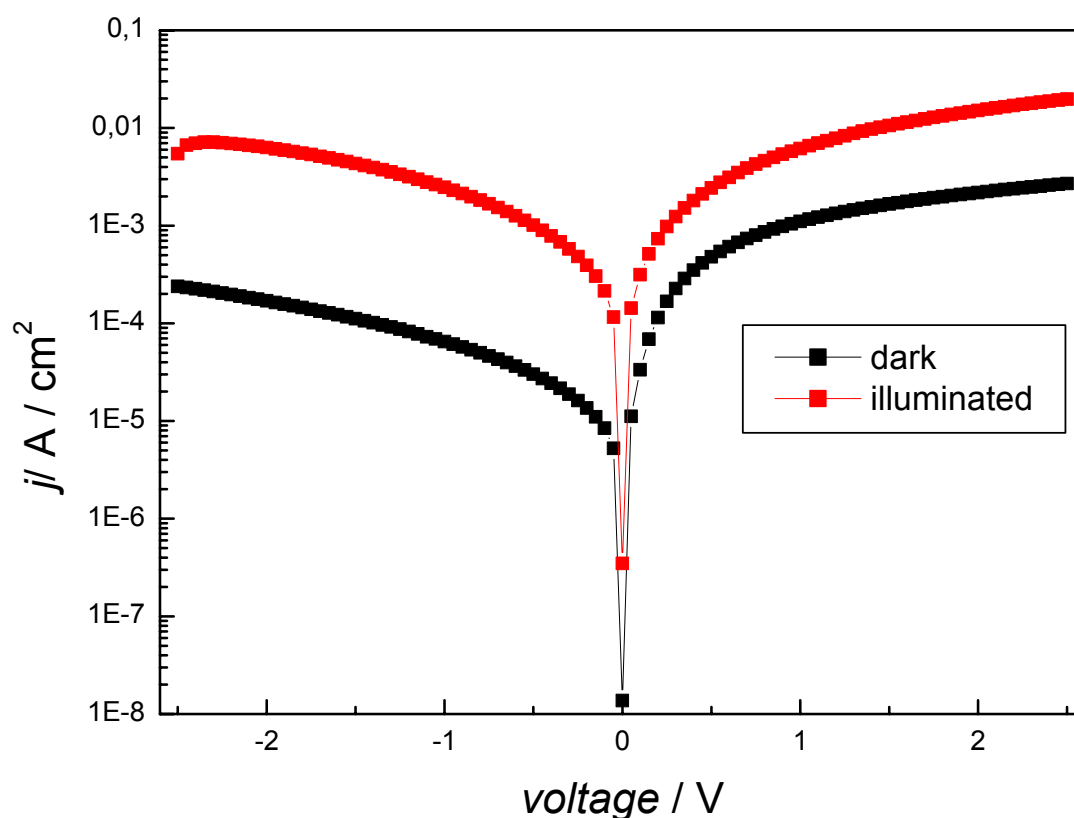


Figure 41: $J - V$ characteristic in logarithmic plot of a ITO glass / CIS / P3HT / Au bilayer solar cell

By comparing the results of the CIS/PCBM and CIS/P3HT bilayer solar cells one can easily see that the results with PCBM are much better. Therefore it seems more promising to work with p-type than with n-type CIS.

3.5.2 Bulk Heterojunction Solar Cells

Due to big problems with the morphology of the samples no results could be achieved. The morphology can be seen in the AFM-pictures in Figure 34 - Figure 36. Nearly all samples were short circuited.

CIS : P3HT

CIS and P3HT were mixed in different weight-ratios: 1 : 1, 3 : 1 and 6 : 1. The concentration of P3HT was 3 wt % in chloroform. To get thick films without shorts the films were dropcast or doctorbladed. The particles were from batch 1.

Most of the cells were very bad and it was not possible to get any cells which were not shorted. There were only few cells with a RR over 10. Therefore it is not possible to say which ratio is the best and if dropcasting or doctorblading is better.

CIS : PCBM

CIS and PCBM were mixed in different weight-ratios (1 : 1, 2 : 1, 4 : 1, 6 : 1, 10 : 1). The concentration of PCBM was 3 wt % in chlorobenzene. The nanoparticles were from batch 2 and 3. The solution was spincoated or dropcast on ITO.

Due to big problems with the morphology of the samples no results were achieved.

3.5.3 CISCuT Solar Cells

The nanoparticles for these cells were taken from batch 4 to form a buffer and window layer [39, 40, 41].

The $J - V$ curves were measured from -1 to 1 V The best cell shows a V_{OC} of 300 mV, j_{SC} of 1.2 mA cm⁻² and a efficiency of 0.11 % (Figure 42).

In comparison to Cu(S,O) buffer layers ($V_{OC} = 653$ mV, $j_{SC} = 16.1$ mA cm⁻², $FF = 0.57$, $\eta = 6.1$ %) [36], PEDOT:PSS buffer layers ($V_{OC} = 543$ mV, $j_{SC} = 11.5$ mA cm⁻², $FF = 0.30$, $\eta = 1.9$ %) [39] or polypyrrole buffer layers ($V_{OC} = 273$ mV, $j_{SC} = 5.52$ mA cm⁻², $FF = 0.23$, $\eta = 0.38$ %) [41]

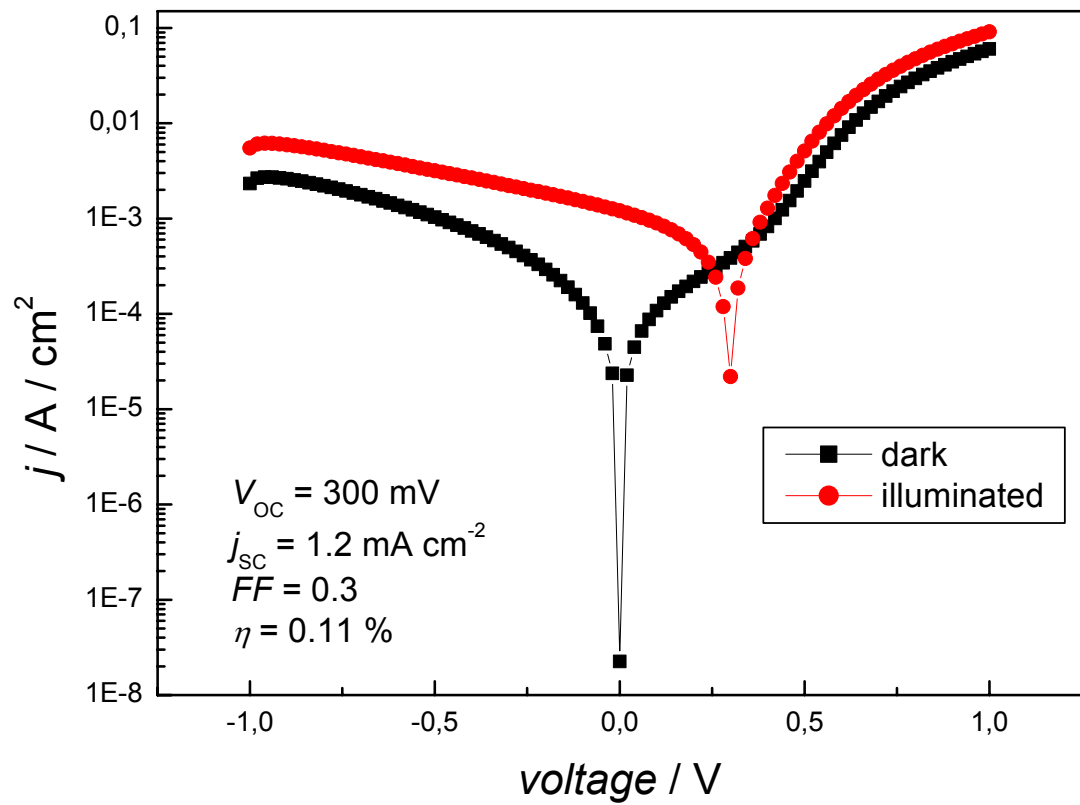


Figure 42: J – V characteristic in logarithmic plot of a CISCuT solar cell with CIS nanoparticles as buffer layer

3.6 IPCE Measurements

As mentioned above IPCE gives the spectral resolution of the photocurrent. Here (Figure 43) the IPCE measurement of a bilayer solar cell of CIS / PCBM and the absorption of a dropcasted CIS film on ITO glass are compared. It shows that mixing the two compounds has a big effect on the absorption.

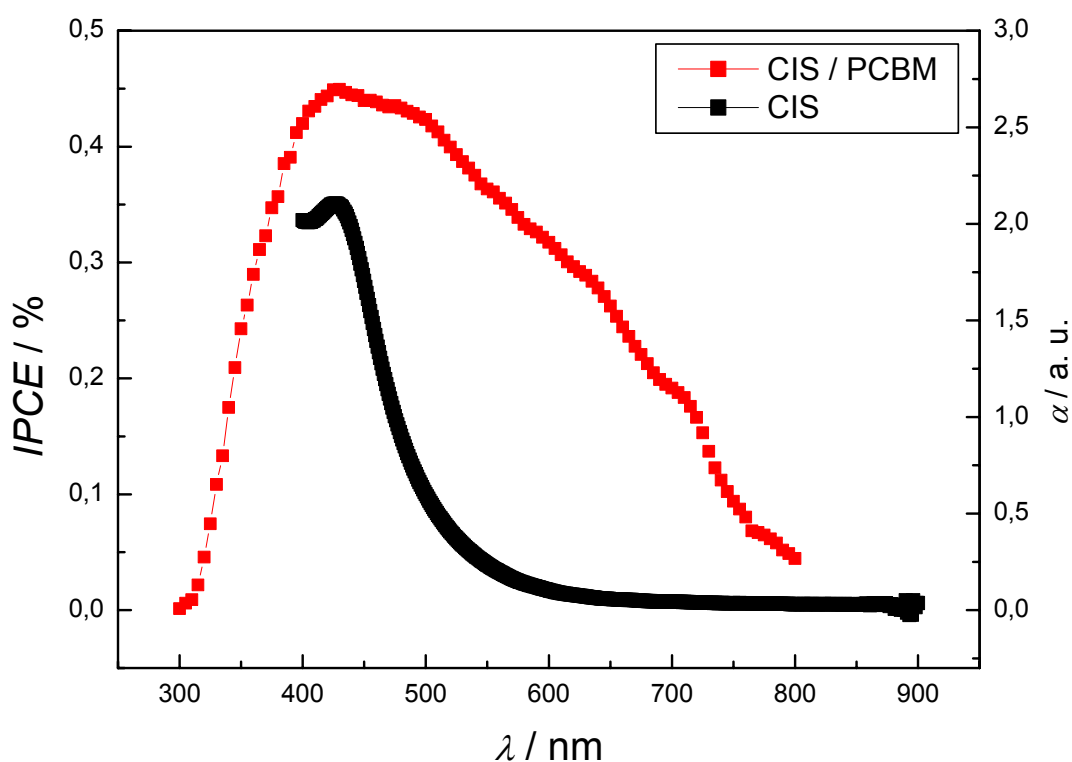


Figure 43: IPCE-spectrum of a CIS / PCBM bilayer solar cell and the absorption of a dropcasted CIS film on ITO glass

4 Conclusion

CIS nanoparticles were synthesised via the colloidal route. The characteristics of the nanoparticles varied by changing the parameters of the synthesis. We observed that the amount of sulphur added played a role on the type of conductivity of the particles. P-type conductivity was achieved when sulphur was added in a stoichiometric ratio whereas n-type conductivity was achieved by increasing the amount of sulphur. Therefore it was possible to build on the one hand hybrid solar cells using CIS as an electron acceptor and P3HT as hole transporters and on the other hand hybrid solar cells with CIS as hole transporters and PCBM as electron transporters, depending on the type of conductivity of the nanoparticles. With p-type CIS better results for solar cells were achieved.

The particles were characterised by using X-ray analysis, transmission electron microscopy (TEM) and atomic force microscopy (AFM).

X-ray analysis confirmed that CIS nanoparticles were obtained by using this colloidal route.

The morphology of the nanoparticles was analysed by using TEM and AFM.

TEM revealed that CIS nanoparticles have both crystalline and amorphous phases. AFM investigations showed that all films of CIS nanoparticles have a high surface roughness which led to inhomogeneous and incomplete film structure that caused short circuits in the cells prepared.

Even though the RR's were better than for the cells published by Arici et al. [8, 15], the other cell parameter like V_{OC} , j_{SC} , fill factor and efficiency were lower compared to the same unit of other hybrid solar cells.

Investigations on using CIS nanoparticles as buffer layer in CISCuT solar cells showed a maximal efficiency of 0.1 %. But in comparison to Cu(S₂O) buffer layers [39], PEDOT:PSS buffer layers [42] or polymerepolypyrole buffer layers [44] CIS nanoparticles do not seem to be the best choice for a buffer layer.

Overall, CIS nanoparticles were successfully synthesised via a colloidal route. The low power conversion efficiencies of the hybrid solar cells investigated is an indication that the morphology problems and surfactants are still limiting factors

and these problems may be overcome by using more effective synthesis routes like hydrothermal synthesis.

References

- [1] H. Weller, *Angew. Chem. Int. Ed. Engl.*, **32** (1993), 41
- [2] M. L. Steigwald, L. E. Brus, *Acc. Chem. Res.*, **23** (1990), 283
- [3] A. P. Alivisatos, *Science*, **271** (1996), 933
- [4] S. A. Empedocles, M. G. Bawendi, *Acc. Chem. Res.*, **32** (1999), 389
- [5] C. J. Murphy, J. L. Coffey, *Appl. Spectr.* **56** (2002), 16
- [6] N. C. Greenham, X. Peng, A. P. Alivisatos, *Phys. Rev. B*, **54** (1996), 17 628 – 17 637
- [7] E. Arici, H. Hoppe, F. Schäffler, D. Meissner, M. A. Malik, N. S. Sariciftci, *Appl. Phys. A*, **79** (2004), 59 – 64
- [8] E. Arici, H. Hoppe, F. Schäffler, D. Meissner, M. A. Malik, N. S. Sariciftci, *Thin Solid Films*, **451 – 452** (2004), 612 – 618
- [9] W. U. Huynh, W. W. Dittmer, A. P. Alivisatos, *Science*, **295** (2002) 2425
- [10] E. Arici, D. Meissner, F. Schäffler, N. S. Sariciftci, *International Journal of Photoenergy*, **5** (2003), 199-208
- [11] J. J. Loferski, Non-Stoichiometric Semiconductors, Proc. Symp. A3 Int. Conf. Adv. Mater. (1992), 257-68
- [12] E. Arici, N. S. Sariciftci, D. Meissner, *Adv. Funct. Mater.*, **13** (2003), 1 – 7
- [13] H. Hoppe, N. S. Sariciftci, *J. Mater. Res.*, **19** (2004), 1924 – 1944

- [14] B. A. Greeg, M. C. Hanna, *J. Appl. Phys.*, **93** (2003), 3605
- [15] S. M. Sze: *Physics of Semiconductor Devices*, John Wiley & Sons, New York (1981)
- [16] M. Murgia, F. Biscarini, M. Cavallini, C. Taliani, G. Ruani, *Synth. Met.*, **121** (2001), 1533
- [17] P. Peumann, A. Yakimov, A. R. Forrest, *J. Appl. Phys.*, **93** (2003), 3693
- [18] L. A. A. Petterson, L. S. Roman, O. Inganäs, *J. Appl. Phys.*, **86** (1999), 487
- [19] C. W. Tang, *Appl. Phys. Lett.*, **48** (1986), 183
- [20] J. Rostalski, D. Meissner, *Sol. Energy Mater. So. Cells*, **63** (2000), 37
- [21] L. Smilowitz, N. S. Sariciftci, R. Wu, C. Gettinger, A. J. Heeger, F. Wudl, *Phys. Rev. B*, **47** (1993), 13835
- [22] G. Ruani, C. Fontanini, M. Murgia, C. Taliani, *J. Chem. Phys.*, **116**, (2002), 1713
- [23] T. Toccoli, A. Boschetti, C. Corradi, L. Guerini, M. Mazzola, S. Iannotta, *Synth. Met.*, **138** (2003), 3
- [24] V. I. Arkhipov, P. Heremans, H. Bässler, *Appl. Phys. Lett.*, **82** (2003), 4605
- [25] N. S. Sariciftci, A. J. Heeger, in *Handbook of Organic Semiconductive Molecules and Polymers*, Vol. 1, edited by H. S. Nalwa, John Wiley & Sons Ltd. Chichester, UK, (1997), 413
- [26] A. F. Nogueira, I. Montari, J. Nelson, J. R. Durrant, C. Winder, N. S. Sariciftci, C. Brabec, *J. Phys. Chem. B*, **107** (2003), 1567

- [27] A. J. Breeze, A. Salomon, D. S. Ginley, B. A. Gregg, H. Tillmann, H.-H. Hörhold, *Appl. Phys. Lett.*, **81** (2002), 3085
- [28] C. J. Brabec, N. S. Sariciftci, J. C. Hummelen, *Adv. Funct. Mater.*, **11**, (2001), 15 – 26
- [29] S. Shaheen, C. J. Brabec, F. Padinger, t. Frommherz, J. C. Hummelen, N. S. Sariciftci, *Appl. Phys. Lett.*, **78** (2001), 841
- [30] C. Czekelius, M. Hilgendorff, L. Spanhel, I. Bedja, M. Lerch, G. Müller, U. Bloeck, D.-S. Su, M. Giersig, *Adv. Mater.*, **11** (1999), 643 – 646
- [31] X. Peng, L. Manna, W. Yang, J. Wickham, E. Scher, A. Kadavanich, A. P. Alivisatos, *Nature*, **404** (2000), 59 – 61
- [32] D. V. Talapin, R. Koeppel, S. Götzinger, A. Kornowski, J. M: Lupton, A: L. Rogach, O. Benson, J. Feldmann, H. Weller, *Nano Lett.*, **3** (2003), 1677 – 1681
- [33] C. Mitterbauer, *Herstellung und Charakterisierung von Bariumtitanat-, Strontiumtitanat- und Magnesiumoxidschichten auf texturiertem Titan*, Diplomarbeit am Institut für Chemische Technologie Anorganischer Stoffe, Johannes Kepler Universität, Linz, (2005), 34 - 35
- [34] G. M. Barrow, *Physikalische Chemie*, 6. Auflage, Böheimverlag, Wien (1984), 109 – 110
- [35] <http://www.unl.edu/CMRAcfem/temoptic.htm> (13. 06. 2005)
- [36] J. Penndorf, M. Winkler, O. Tober, D. Röser, K. Jacobs, *Sol. Energy Mater. Solar Cells*, **53**, (1998), 285 – 298
- [37] T. M. Brown, R. H. Friend, I. S. Millard, D. J. Lacey, T. Butler, J. H. Burroughes, F. Cacialli, *J. Appl. Phys.*, **93** (2003), 6159 – 6172

- [38] C. J. Brabec, S. E. Shaheen, C. Winder, N. S. Sariciftci, P. Denk, *Appl. Phys. Lett.*, **80** (2002), 1288 - 1290
- [39] S. Bereznev, I. Konovalov, J. Kois, E. Mellikov, A. Öpik, *Mat. Res. Soc. Symp. Proc.*, **771**, (2003), 243 – 248
- [40] M. Winkler, J. Griesche, I. Konovalov, J. Penndorf, J. Wienke, O. Tober, *Sol. Energy*, **77** (2004), 705 – 716
- [41] S. Bereznev, I Konovalov, A., Öpik, J. Kois, E. Mellikov, *Sol, Energy Mat. & Solar Cells*, **87** (2005), 197 - 206

Curriculum Vitae



Name: Sandra Martina Hofer
Date of Birth: 7. 3. 1980
Birthplace: Vienna
Nationality: Austrian
Marital Status: Single

Education

06/ 2004 – 07 / 2005 Diploma Thesis at the institute for physical chemistry, Prof. Mag. Dr. S. N. Sariciftci,
02 / 2005 Start of additional education: Economics
1998 - 2005 Studies at the University of Linz:
Economical engineering of technical chemistry
06 / 1998 School leaving exam passed with distinction, scholarly paper, chemistry,
Dr. Wluszczak,
„HI-Virus und AIDS - Die Biochemie des Virus, sein Nachweis und neueste Methoden der Therapie“ (HI-Virus and AIDS – Biochemistry and Detection of the Virus and new Methods of Therapy)
1990 – 1998 Grammar school in Unterwaltersdorf, NÖ
1986 – 1990 Primary school in Vienna

Practical Experience:

- 02 -03 /2004 project collaborator at the institute of physical chemistry
- Summer 2001, 2002, 2003 internship Novartis Forschungs Institut, Vienna, Lab Dr. B.Wolff-Winiski: operations in the field of molecular biology
- Summer 1999, 2000 internship Novartis Forschungs Institut, Vienna, Lab Dr. P. Etmayer: operations in the field of organic preparative chemistry

Further Employers:

- 11 /2001 – 09 / 2002 Dekanat der Technisch Naturwissenschaftlichen Fakultät, Linz, project collaborator at FIT
- Summer 1996, 1998, 1999 Centro Internationale Handelsbank, Vienna, Department Processing
- Summer 1995 Gerot Pharmazeutika, Vienna: Department Stock

Additional Qualifications

- Good command of English (spoken and written)
- Driver's licence since 1998
- German Flute

Hobbies

- Ice- and inline hockey, skiing, travelling

Eidesstattliche Erklärung

Ich erkläre an Eides statt, dass ich die vorliegende Diplomarbeit selbstständig und ohne fremde Hilfe verfasst, andere als die angegebenen Quellen und Hilfsmittel nicht benutzt, bzw. die wörtlich oder sinngemäß entnommenen Stellen als solche kenntlich gemacht habe.

Linz, am